

AD-A239 802

SBI/NORDA

2



Naval Ocean Research and Development Activity

January 1990

Report 209

e040097

An Analysis of Surface-duct Propagation Loss Modeling in SHARPS

DTIC  
ELECTE  
AUG 22 1991  
S B D

Robert W. McGirr  
Numerical Modeling Division  
Ocean Acoustics and Technology Directorate

91-08367



Approved for public release; distribution is unlimited. Naval Ocean Research and Development Activity, Stennis Space Center, Mississippi 39529-5004.

91 8 20 112

## Foreword

---

The Fleet Numerical Oceanography Center is chartered to generate daily forecasts of detection range for ASW sonar systems that operate in a wide variety of ocean environments. This report reviews the surface-duct propagation loss prediction capabilities of the Ship Helicopter Acoustic Range Prediction System.

*William B Moseley*

**W. B. Moseley**  
**Technical Director**

*J. B. Tupaz*

**J. B. Tupaz, Captain, USN**  
**Commanding Officer**

# Executive Summary

---

The propagation submodels of the Ship Helicopter Acoustic Range Prediction System (SHARPS) are reviewed within the context of their effectiveness in making accurate predictions for surface-duct environments. The surface-duct propagation loss calculations performed by SHARPS are based on the submodels contained in Active RAYMODE. Fleet messages have been critical of SHARPS target detection range predictions for in-layer and cross-layer sonar-target geometries. A review is presented of those computational methods—common to both Active and Passive RAYMODE—most likely to affect surface-duct predictions, and includes a summary of the main features of a surface-duct leakage subroutine found in one of the previous versions of Passive RAYMODE. A means of coupling surface-scattered energy into the normal mode sum is reviewed. The possibility of “anomalous” surface-duct predictions is briefly addressed, and several ways to achieve improved surface-duct propagation loss predictions are recommended.



|                    |                                     |
|--------------------|-------------------------------------|
| Accession For      |                                     |
| NTIS GRA&I         | <input checked="" type="checkbox"/> |
| DTIC TAB           | <input type="checkbox"/>            |
| Unannounced        | <input type="checkbox"/>            |
| Justification      |                                     |
| By _____           |                                     |
| Distribution/      |                                     |
| Availability Codes |                                     |
| Dist               | Avail and/or Special                |
| A-1                |                                     |

## Acknowledgments

---

The author wishes to express his appreciation to Dr. David King of the Naval Ocean Research and Development Activity (NORDA) for his technical review and helpful suggestions, to Mr. Curtis Favre for making model runs, and to LCDR Chris Hall of the Fleet Numerical Oceanography Center and Mr. Eigo Hashimoto of NORDA (FNOC Liaison) for their encouragement and support. The work reported herein was sponsored by FNOC's ASW Tactical Support Division, Program Element 980101.

# Contents

---

|  |    |
|--|----|
| <b>I. Introduction</b>   | 1  |
| <b>II. A Review of RAYMODE Model Physics</b>   | 2  |
| A. Methods Used in Passive RAYMODE   | 2  |
| B. Original RAYMODE Integration  | 3  |
| C. Special High-frequency Integration  | 3  |
| D. Surface Reflection Loss   | 4  |
| <b>III. Surface-duct Propagation Modeling</b>  | 4  |
| A. RAYMODE Surface-duct Model  | 4  |
| B. Characteristics of the Bilinear Profile Model                                     | 7  |
| <b>IV. Coupling of Surface Scattered Energy</b>                                      | 9  |
| <b>V. Computational Artifacts</b>  | 11 |
| <b>VI. Summary Remarks</b>   | 12 |
| A. Conclusions   | 13 |
| B. Recommendations   | 15 |
| <b>VII. References</b>   | 16 |
| <b>Appendix A: Normal-mode and Multipath Expansion Forms</b>                         | 19 |
| <b>Appendix B: Special RAYMODE Integration</b>                                       | 31 |
| <b>Appendix C: Breakdown of Phase Factor</b>   | 37 |
| <b>Appendix D: Surface Reflection Loss Submodel</b>                                  | 43 |
| <b>Appendix E: Complex Eigenvalues</b>   | 47 |
| <b>Appendix F: Departure of <math>n^2</math>-linear Profile Model from Linearity</b> | 51 |
| <b>Appendix G: Modal Parameters for a <math>C^3</math>-linear Duct</b>               | 55 |
| <b>Appendix H: Bucker's Scattering Integrals</b>                                     | 59 |

# An Analysis of Surface-duct Propagation Loss Modeling in SHARPS

---

## I. Introduction

This report presents a qualitative assessment of the surface-duct propagation loss prediction capability of the Ship-Helicopter Acoustic Range Prediction System (SHARPS). SHARPS is used by the Fleet Numerical Oceanography Center (FNOC) to generate daily forecasts of detection ranges for several operational sonar systems. The Active RAYMODE model generates the basic acoustic quantities used by the latest version of SHARPS. The propagation loss subroutines of Active RAYMODE were derived from Passive RAYMODE, the latter being the new Navy standard propagation loss model for range-independent ocean environments. Since the installation of Active RAYMODE in SHARPS, FNOC has received messages critical of "anomalous" detection range predictions under certain surface-duct conditions.

Passive RAYMODE has been declared the Navy standard propagation loss model for range-independent ocean environments. As a consequence, all propagation loss modules used in generating fleet prediction products had to be changed to meet the new standard. The decision was made that even though such changes would be extremely costly, the costs were worth the desired result: commonality of all propagation loss modules used in generating fleet prediction products. Thus, both the Active and the Passive versions of RAYMODE have been (or are being) installed at FNOC to provide the basic transmission loss calculations used in several fleet performance prediction systems.

The specific prediction system of interest here is SHARPS. This system was developed at FNOC in the late 1960s. In its original form, SHARPS was purely empirical. In the early 1970s, SHARPS was completely revised in an effort to incorporate the physics of under water sound. An attempt to use the original version of the Navy Interim Surface Ship Model (NISSM) failed due to unacceptable run-times. A trimmed version of NISSM, referred to simply as FAST NISSM (Watson and McGirr, 1972; McGirr, et al., 1972), was finally installed for operational use in 1973. This code (then identified as SHARPS II) had many shortcomings and was replaced in 1977 by a

"streamlined" version of NISSM II (Weinberg, 1973; Kirby, 1982). From that point until 1986 this version of the SHARPS model (then identified as SHARPS III) underwent numerous upgrades.

One of the major problems with both SHARPS II and SHARPS III centered on the surface-duct model (based on the AMOS equations in both versions) and, in particular, the procedure used in defining the sonic-layer depth (for an amplification of this problem, see McGirr, 1983). The sonic layer depth problem was never satisfactorily resolved. Indeed, the analyses of Renner and Kirby (1983) revealed that a pre-SHARPS profile-processing program occasionally yielded erroneous surface-duct parameters. This problem, in combination with an overly simplified treatment of surface-duct propagation, resulted in unacceptably large swings in detection range whenever the near-surface velocity gradients were exceptionally close to zero.

Virtually the same problem exists with the new version of SHARPS, except that no special treatment is given to surface-duct propagation. The near-surface propagation loss prediction problems that existed in previous versions of SHARPS were expected to disappear with the installation of Active RAYMODE. This supposition evidently emerged from expectations that the "modal" character of the new propagation code would automatically take interduct coupling into account, thereby precluding any need for a surface-duct submodel. These expectations were soon replaced by expressions of concern, however, once the message traffic revealed the reality of the situation: the "normal mode" method used in Active RAYMODE essentially ignores the coupling of energy from one duct to another. Thus, the surface-duct problem persists, and FNOC personnel once again find themselves trying to respond to criticisms from the Fleet regarding the "same old problem."

Essentially, recipients of SHARPS forecasts question in-layer and cross-layer detection range predictions. For presumably well-defined surface ducts, predicted detection ranges for both sonar and target in the duct are shorter than detection ranges predicted for sonar in the duct and target below the duct. However,

on-board predictions for the same inputs yield the opposite results. The first question is, were identical inputs used by both the ashore and the afloat prediction systems? The second question is, are both the ashore and the afloat implementations of the basic acoustic model (namely, Active RAYMODE) identical?

The first question can be answered only by Fleet and FNOC personnel responsible for making the predictions. The second question, however, brings up implementation issues. Both Active and Passive RAYMODE are under configuration management and, as part of each software package, test cases are included for verification. Presuming that the Active RAYMODE software was verified after being hard-wired into the SHARPS "shell" and that a similar verification procedure is faithfully followed after installation in each system afloat, the logical course of action entails comparing surface-duct predictions generated by ashore and afloat version of Active RAYMODE against high-confidence control models. If acceptable agreement is not obtained by either version, then the only recourse is to analyze the physics contained in Active RAYMODE that deals with surface-duct environments.

The verification procedure alluded to above may not uncover "bugs" peculiar to implementations on specific machines or operating systems. Steps have been taken by both the developing agency, the Naval Underwater Systems Center (NUSC), and the organization responsible for configuration management, Naval Oceanographic Office (NAVOCEANO), to ensure that there is no machine/operating-system dependency. The RAYMODE codes delivered to the Naval Ocean Research and Development Activity (NORDA) were programmed in strict FORTRAN 77, which should be free of any such dependencies. Nonetheless, there is always the possibility that a model which generates acceptable results on the HP-9020/UNIX will not, for some cases, generate identical results on a VAX running VMS. Even though there may be some questions regarding verification, which are presumably being addressed by the various software firms involved, the purpose of the effort reported herein is to uncover weaknesses in the Active-RAYMODE model with regard to surface-duct predictions.

The report is broken down into four major sections. Section II reviews those aspects of the RAYMODE physics modeling that might have some bearing on surface-duct predictions. Section III addresses surface-duct propagation modeling problems in general. Section IV examines the impact of neglecting surface scattered energy. Section V illustrates jump discontinuities that are common to methods based on hybrid solutions, and Section VI closes the report with summary remarks and recommendations.

## II. A Review of RAYMODE Model Physics

Passive RAYMODE was initially conceived in the late 1960s by Leibiger (1968) and has evolved into a widely used propagation code. In essence, Leibiger replaces the single contour integral of the Fourier-Bessel solution to the reduced wave equation into several integrals, each of which can be associated with a family of rays. These integrals, which result from expanding the reciprocal of the Wronskian into an infinite series, are then evaluated using an approximate normal-mode method if the number of modes is not too large or otherwise using integration techniques more-or-less unique to RAYMODE. The advantages offered by RAYMODE over standard normal-mode treatments are two-fold. First, the computational load does not significantly increase with increasing frequency, as is the case with normal-mode models. Second, the solution is partitioned into components that give rise to plausible geometrical interpretations similar to those available from methods based strictly on ray acoustics.

The propagation-loss algorithms used in Active RAYMODE essentially form a subset of those used in Passive RAYMODE. As a consequence, Active RAYMODE users are concerned about the loss in accuracy that could result from calculations restricted to the high-frequency algorithms of Passive RAYMODE. Concerns of the same sort also pertain to Passive RAYMODE, since numerous assumptions and approximations have been made in an effort to obtain fast execution times. The focus here is on those aspects of RAYMODE that potentially impact surface-duct predictions.

### A. Methods Used in Passive RAYMODE

Certain documents (Leibiger, 1968, 1971; Deavenport, 1978; Davis and Council, 1985a, 1985b) present various aspects of the model physics. The text by DiNapoli and Deavenport (1979) is an excellent reference on contemporary propagation modeling in general, and also presents a brief discussion of RAYMODE. Those documents written by Davis and Council are the most complete, although the sections that address the special surface-duct treatment do not apply to the most recent version of Passive RAYMODE, since the surface-duct module is not included in the latest version. Moreover, this surface-duct treatment evidently has never been considered for inclusion in Active RAYMODE.

The steps leading to the RAYMODE versions of normal-mode and multipath expansion solutions are developed in Appendix A. Much of the material presented in Appendix A parallels the Passive RAYMODE documentation of Davis and Council (1985b). Readers who are interested in understanding the model physics should peruse all of the references.

For surface-duct paths, three RAYMODE methods can be applied to solve the multipath expansion integral, although the surface-duct option offered in a previous version of RAYMODE essentially represents a fourth RAYMODE method. The other three methods are (1) numerical integration based on the fast, Fourier transform (FFT); (2) the original RAYMODE integration (ORI) method; and (3) a special high-frequency integration (HFI) method. If the user does not select a particular method, then the program selects one. For frequencies less than 3000 Hz, either of the first two methods is selected, depending on estimated execution time for each method. If the best option is the FFT method, but aliasing is anticipated, then the ORI method is used instead. For frequencies greater than 3000 Hz, the special HFI method is selected. The methods of primary interest here are the original RAYMODE integration method and the special HFI method. The special surface-duct treatment that Leibiger applied in a previous version of RAYMODE is discussed in Section III. The ORI and HFI methods are discussed in the next two subsections.

## B. Original RAYMODE Integration

The general form of the RAYMODE multipath expansion\* integral (see Eq. (A38) in Appendix A) is

$$I(k_a, k_b) = \int \beta(k) \exp\{-i[kr + \alpha(k)]\} dk, \quad (1)$$

where the limits of integration extend from  $k_a$  to  $k_b$ . An approach often used in the evaluation of integrals of this form is the method of stationary phase. This method is summarized in Appendix B.

Leibiger interrupts the stationary-phase analytical process and does not actually proceed to the final formula (see Eq. (B51) of Appendix B). The reason for this circumvention is that the conditions required to achieve the final step may not, for all frequencies of interest, be met. An acceptable application of the formula requires that the function in the exponent,  $h(k)$ , be multiplied by a large constant. The constant in the development as presented in Appendix B is unity. The argument of the phase function can be expressed as, for example,  $k_o[kr/k_o + \alpha(k)/k_o]$ , and the variable of integration transformed to  $k/k_o$ , where  $k_o$  ( $= 2\pi f/C_o$ ) is some reference wavenumber. Thus, the stated condition is met for high frequencies. For low frequencies, the limits of integration must be confined to a relatively small interval, where (hopefully) the resulting integral yields an accurate estimate. Early work by Leibiger (1968) indicates that the stationary-phase formula was initially exploited and

then discarded in favor of the method outlined in Appendix B.

Leibiger (1971) demonstrates the relationship between the stationary-phase "formula" and the standard ray-acoustical expression. In an earlier report (Leibiger, 1968), he demonstrates that the existence of a point of stationary phase implies the existence of a ray trajectory connecting the source and the receiver.

The ORI method, as presented in Appendix B, suggests the not entirely implausible possibility that the amplitude and phase factors do not necessarily accede to conditions generally assumed extant in justifying the application of stationary-phase methods. These matters are discussed in Appendix C. Even when the evaluation occurs at an end point, a stationary phase analysis can be used successfully to determine asymptotic behavior. A precise assessment of the impact of asymptotic behavior is beyond the scope of this effort, but as a practical matter, in any problem where a function is to be approximated, some a priori upper bound is placed on the tolerable error. A perusal of the computer code indicates that Leibiger has taken precautionary steps to circumvent serious problems.

Some hint about the magnitude of error attributable to the ORI method can be gleaned from Bartberger's (1981) evaluation of a previous version of Passive RAYMODE. Bartberger notes that differences between the normal-mode method and the ORI method (which may have been altered since) can be significant for coherently summed outputs but appear to be minor for incoherently summed outputs. Discontinuous jumps that are created when the method of solution switches from one form to another are briefly examined in Section IV.

Leibiger (1971) notes that his particular stationary-phase treatment avoids certain problems that can develop as the acoustic frequency increases. At a high enough frequency, the ORI method is supplemented by a special high frequency integration HFI approach.

## C. Special High-frequency Integration

Keep in mind that a derivation of the high-frequency procedure has not been documented by the model developer, so the only information available is the brief description given by Davis and Council (1985b), and the computer code. The main features of this technique are presented in Appendix B.

A perusal of the computer code for details on how the HFI procedure is implemented reveals that the Airy integral is approximated by a polynomial of degree six when the argument has magnitude less than five, and by the inverse square of the argument otherwise. This particular form of asymptotic representation seems rather crude, although quite possibly justified. The polynomial approximation appears to be a truncated power series expansion, which probably can be

\*For an elementary interpretation of this technique consult Sect. 35 in the text by Brekhovskikh (1980).

improved upon by using an economized rational polynomial approximation instead.

#### D. Surface Reflection Loss

RAYMODE surface reflection loss calculations are based on an ad hoc adaptation of results derived in part from theoretical considerations and in part from experimental data (Marsh and Schulkin, 1962). A summary of this submodel is presented in Appendix D.

### III. Surface-duct Propagation Modeling

This section addresses several more or less independent aspects of modeling propagation loss for surface-duct environments. One of the working hypotheses upon which this report is based is that the surface-duct model used in the 1983 version of RAYMODE can, with suitable modifications, yield improved surface-duct predictions if incorporated into the latest versions of the RAYMODE codes. Modifications are necessary for two reasons: there appear to be errors in the computer code and some means should be incorporated to account for the coupling of surface-scattered energy into the below-layer region. This latter topic is addressed in Section IV.

The RAYMODE special surface-duct algorithms alluded to are discussed in Section A. Section B presents some characteristics of the two-segment  $n^2$ -linear velocity profile model, which forms the basis of the surface-duct module used in the latest versions of FACT and ASTRAL. This approach to the problem has both advantages and disadvantages. A procedure that was successfully used in the 1960s is reviewed, and several detracting features of the  $n^2$ -linear model are discussed.

#### A. RAYMODE Surface-duct Model

The normal-mode sum used in Active RAYMODE is possibly adequate to handle range-invariant, shallow-water ducts. For deep-ocean profiles that contain multiple ducts, there is no provision for cross-channel coupling. Also, the mode sum is limited to a maximum of 10 propagating modes, so for frequencies above about 3 kHz most ducts are likely to be handled by the HFI method. In many normal-mode codes, the modes (eigenvalues) are determined by numerical integration over the entire water column. Some codes use iterative procedures to solve the characteristic equation. In either case, interchannel coupling effects are automatically included. The simplified procedure used in Active RAYMODE, as it stands, cannot address this type of coupling.

The 1983 version of Passive RAYMODE includes the option of a special treatment of the normal-mode method when applied to surface ducts. In the standard RAYMODE approach, the magnitude of the reflection coefficient at each k-segment interface is one,

except at the surface and the bottom. In the special treatment accorded surface ducts, generalized Wentzel-Kramers-Brillouin (WKB) reflection coefficients are introduced. These reflection coefficients are then used in constructing complex eigenvalues, where each imaginary component corresponds to an exponential loss of energy with range. Thus, for a source located within the duct, WKB modes lose some of their energy at each turning point, where the lost energy is transmitted into the region below the layer depth. Similarly, modes excited by a source located in the negative-gradient region transfer some of their energy to waves that propagate within the duct. This procedure, if added to the present version of Active RAYMODE, should yield improved estimates of surface-duct propagation. To have any impact at frequencies above, say, 3 kHz, the maximum number of modes would have to be extended to about 50. Thus, questions naturally arise pertaining to run-time and accuracy required in the determination of the complex eigenvalues.

The only documentation on the basis for this special surface-duct procedure is the brief account presented by Davis and Council (1985b). (The generalized WKB reflection coefficient procedure is described in the article by Murphy and Davis, 1974) The modifications to the mode sum depend on source-receiver geometry. When both the source depth ( $z_s$ ) and the receiver depth ( $z_r$ ) are less than the layer depth ( $z_L$ ), the mode sums are applicable using appropriate reflection coefficients at the turning points. The upper turning point in this case is the surface; therefore,  $R_u$  corresponds to the surface reflection coefficient (discussed in Appendix A). At the lower turning point depth, say,  $z_l$ ,  $R_l$  is replaced by  $R_{AB}(z_l)$ , a generalized WKB reflection coefficient. The subscript, AB, indicates the sense of direction associated with the coefficient, where A stands for above-layer and B stands for below-layer. Details pertaining to the calculation of this coefficient, along with the corresponding transmission coefficient, are presented in subsequent paragraphs.

When both the source and the receiver are situated below the layer depth, the reflection coefficient at the upper turning point is replaced by  $R_{BA}(z_u)$ , which is similar to  $R_{AB}(z_l)$  for the in-layer case, but where the above-layer and below-layer parameters are interchanged. The lower turning point is assumed to be at depth; therefore,  $R_l$  is assumed to have a magnitude of 1 and a phase of  $-\pi/2$ .

For the cross-layer case, say,  $z_s < z_L$  and  $z_r > z_L$ , Leibiger takes a different approach. Instead of reflection coefficients, the amplitude factors are multiplied by a transmission coefficient. Thus, energy that would otherwise be considered trapped using WKB modes, if indeed they even existed, now would have the potential of leaking into the below-layer region.

The "mode-leakage" phenomenon is perhaps best explained by drawing upon ray analogies. Figure 1 illustrates a ray trajectory that turns around at the layer depth. To indicate that some of the energy carried by the ray remains within the duct and that some leaks into the negative gradient region below, the ray is split into two components at the turning point.

To extend the ray analogy a bit further, there are partial reflections at the ray turning points. If  $U_i$  and  $V_i$  denote, for layer  $i$ , two linearly independent solutions of the depth-separated wave equation, then at the layer depth (see Bucker, 1980),

$$U_1 + R V_1 = T U_2, \quad (2)$$

where  $U_1$  and  $V_1$  denote down-going and up-going waves within the duct (layer 1) and  $U_2$  denotes a down-going wave in the region below the duct (layer 2). The reflection and transmission coefficients at the bottom of the duct may be obtained from Ryan (1980):

$$|R|^2 = (1 + s^3)/(1 + s)^3 \quad (3)$$

and

$$|T|^2 = 1 - |R|^2, \quad (4)$$

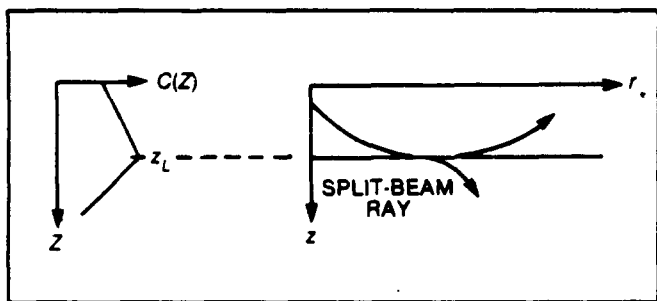


Figure 1. Ray trajectory splitting at layer depth.

where  $s^3 = \beta_1/\beta_2$ . The parameters  $\beta_1$  and  $\beta_2$  are the gradients of the squared index of refraction for each layer (see Fig. 2). Since  $1 + s^3 = (1 + s)(1 - s + s^2)$ , the expression for  $|R|$  can be written

$$R = (1 - s + s^2)^{1/2}/(1 + s). \quad (5)$$

Thus, the transmission coefficient is given by

$$|T| = (3s)^{1/2}/(1 + s). \quad (6)$$

These expressions for  $|R|$  and  $|T|$  are in the forms presented in the RAYMODE documentation of Davis and Council (1985b). Coefficients of the same basic form can be found in the 1983 RAYMODE computer code, although the definition of  $s$  found there is proportional to the reciprocal of the one defined here.\*

Figure 3 indicates the ways (excluding surface scattered paths) in which energy can propagate from an in-layer source to a below-layer receiver. Figure 3 (a) depicts, in terms of ray equivalents, an in-layer trapped mode and a below-layer untrapped mode. These modes interact by means of diffraction leakage through the barrier of thickness  $d = z_l - z_u$ . Figure 3 (b) illustrates the split-beam ray, corresponding to transitional modes, or those modes that are neither strongly trapped nor decidedly leaky. Figure 3 (c) shows a steep ray that, in standard ray-acoustical treatments, transits directly into the below-layer region.

The inclusion of a reflected component is indicative of the situation associated with a leaky mode. Davis and Council (1985v) point out that a generalized

\*This circumstance is a good example of why the physics of a model, especially one intended for operational applications, should be fully documented and subjected to peer review.

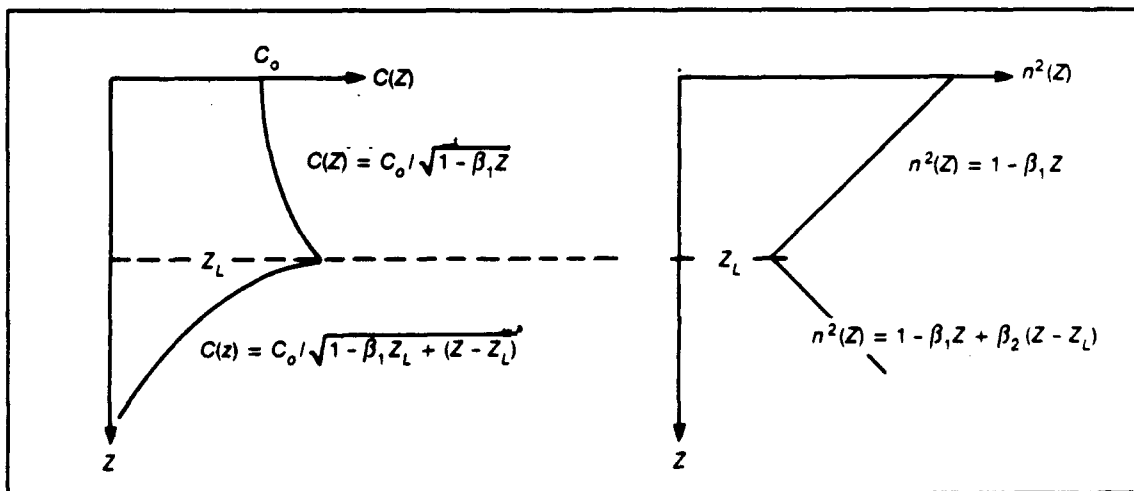


Figure 2. An  $n^2$ -linear profile for two-layer surface duct (a) sound-velocity profile and (b) index-of-refraction profile.

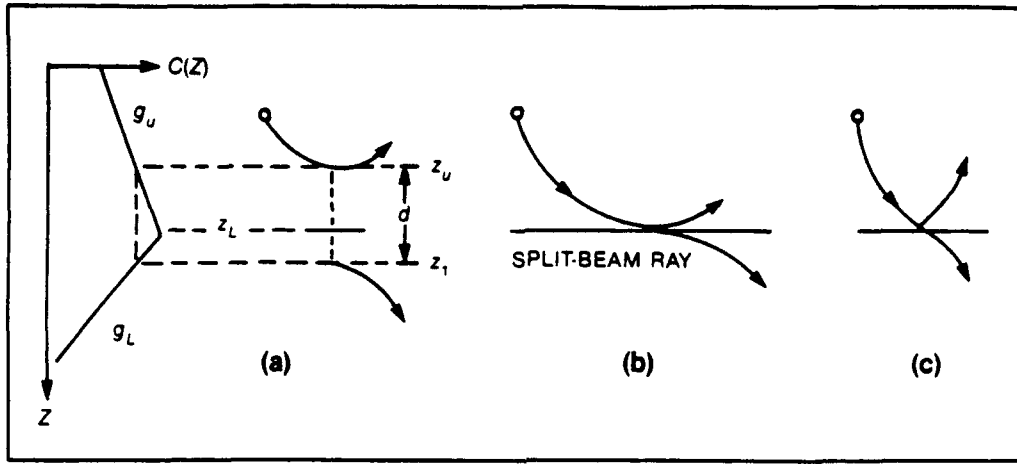


Figure 3. Three direct cross-layer paths.

WKB phase integral approach, if implemented properly, can be used to simulate the interduct energy-coupling process. The reader interested in more details concerning generalized WKB procedures should consult Murphy and Davis (1974). The approach used in Passive RAYMODE is somewhat involved, but essentially a curve is developed that gives  $|R|$ , and therefore  $|T|$ , as a function of in-layer and below-layer parameters defined by

$$\text{(in-layer)} \quad x_1 = h_1^2(k_L^2 - k_m^2), \quad (7)$$

and

$$\text{(below-layer)} \quad x_2 = h_2^2(k_m^2 - k_L^2), \quad (8)$$

where  $k_m = \omega/C_m$ ,  $k_L = \omega/C_L$ ,  $h_1 = (k_o^2 \beta_1)^{-1/2}$ , and  $h_2 = (k_o^2 \beta_2)^{-1/2}$ .

For untrapped modes (Fig. 3 (c); Ryan, 1980) the reflection coefficient can be expressed as

$$|R| = [(1 + s^3)/(4x_i)^3]^{1/2}, \quad i = 1, 2. \quad (9)$$

A curve-fit can then be made using points generated by this equation evaluated at values of  $k_m$  far removed from  $k_L$ , at the point determined for trapped modes, and at a point ( $0 < z < z_u$ ) within the duct using results based on a WKB approximation.

Specific details of this surface-duct submodel are not available in a "technical description" document as is customary, and hence the curious model user must resort to snooping through the computer program source code. Ordinarily, this procedure leads to satisfactory explanations concerning how the model developer surmounts various implementation problems. In the 1983 version of Passive RAYMODE, the surface-duct calculations are done in subroutine SDUCT. A brief review of this code, however, will

discourage all but the most persistent from pursuing this course of action.

SDUCT is highly convoluted and difficult to interpret. Unraveling parts of this code reveals some curious expressions. For example, one line of the SDUCT subroutine reads

$$RL = 1. - HLD + HLD * RLP.$$

Tracing one particular path through the code leads to the following interpretation of this statement:

$$RL = 1 - (R_1 - 1) \exp \left\{ -4/3 \cdot 2 \frac{\omega}{g_1} \left( 1 + \frac{1}{\rho^3} \right) \left| \frac{k_m}{k_1} - 1 \right|^{3/2} \right\}, \quad (10)$$

where  $R_1 = [1 - \rho + \rho^2]^{1/2} / (1 + \rho)$ ,  $\rho^3 = -g_2/g_1$ ,  $g_1$  and  $g_2$  are the in-layer and below-layer velocity gradients,  $k_m$  is the wave number for mode  $m$ , and  $k_1$  is the wave number associated with the layer depth. The expression for  $R_1$  is identical in form to the expression given previously for trapped modes (except that  $\rho = -1/s$ ).

Using the C-linear velocity profile model, the last factor in the exponent can be interpreted as

$$\left| \frac{k_m}{k_1} - 1 \right|^{3/2} = (g_1/C_m)^{3/2} (z_1 - z_m)^{3/2}, \quad (11)$$

where  $z_1$  is the layer depth and  $(z_m, C_m)$  is the depth-velocity pair at the turning point for mode  $m$ . When  $(g_1/C_m)^{3/2}$  is combined with the leading factors in the exponent, this expression can be put into the form

$$RL = 1 - (R_1 - 1) \exp \left\{ -2/3 k_m \beta_m^{1/2} (1 - s^3) (z_L - z_m)^{3/2} \right\}, \quad (12)$$

where  $\beta_m = 2g_1/C_m$ . The exponent in this last expression bears a curious resemblance to exponents typical of WKB phase-integral functions, except that  $k_0\beta_1^{1/2}$  is usually found in place of  $k_m\beta_m^{1/2}$ . The dependence of this factor on mode number is unexpected and deserves explanation.

Although some of the WKB-type expressions found in subroutine SDUCT are similar in basic form to those found in published work (e.g., Barnard and Deavenport, 1978; Hall, 1976; Kibblewhite and Denham, 1965), there are enough differences to warrant separate documentation. The addition of an upgraded version of SDUCT needs to be considered, because the inclusion of generalized WKB reflection and transmission coefficients is necessary to obtain realistic surface-duct predictions using the RAYMODE normal-mode sum (but, of course, with more modes).

## B. Characteristics of the Bilinear Profile Model

The special surface-duct treatment reviewed in Section A makes use of the  $n^2$ -linear velocity profile model to obtain simple expressions for the generalized WKB reflection and transmission coefficients. This profile model has enjoyed wide use in propagation codes, including those based on ray acoustics and normal-mode theory. Among normal-mode codes that rely on analytical solutions to the z-separated wave equation for each profile layer, the  $n^2$ -linear model yields closed-form solutions that can be expressed in terms of Airy functions or modified Hankel functions of order one-third.

This profile model also results in straightforward evaluations of range and travel-time integrals. Although the C-linear (constant gradient) profile model accedes to simple ray-acoustical expressions, it does not lend itself quite so readily to wave-acoustical computations. Essentially, the  $n^2$ -linear profile model represents a mathematically expedient approach to solving wave-acoustical problems, and is probably satisfactory for many modeling requirements. Some of the advantages and disadvantages of using models based on closed-form solutions vice numerical integration are reviewed in subsection B.1.

Two features of the  $n^2$ -linear profile model detract from its appeal, at least in regard to its appropriateness for surface ducts. One feature is the direction of curvature, which is sometimes just the opposite of that suggested by measured profile data; the other is the extreme discontinuity artificially introduced at the layer depth. This last feature is seldom evident in actual profiles. The impact of these features is discussed in subsections B.2.-B.4.

### 1. Computational Pros and Cons

The bilinear normal-mode model was initially developed by Furry (1945); also see Freehafer, 1951) to solve tropospheric electromagnetic wave propagation

problems. It was adapted for underwater acoustics by Marsh (1950) and later refined by Pedersen and Gordon (1965). The Pedersen-Gordon model was subsequently exploited by Watson and McGirr (1966) as an integral component of a production-oriented performance prediction capability. The primary customers were local (U.S. Navy Electronic Laboratory—NEL) developers of active sonar systems. At that time computer technology had not advanced to a stage where numerical integration of the z-separated wave equation was considered a viable option. The two-layer normal-mode model, however, offered some promise as a computationally practicable approach to solving the surface-duct propagation problem.

The characteristic equation associated with this model takes the form of a 3x3 matrix having elements expressible in terms of modified Hankel functions of order one-third\*. These functions were the object of intensive investigation by personnel at the Harvard University Computation Laboratory (1945) during World War II. Their efforts produced extensive tables valuable for verifying independently developed computer algorithms, which provide useful information regarding power-series and asymptotic-series representations of the Hankel functions. Thus, with much of the computational ground work already accomplished, incentive to develop a semiautomated surface-duct propagation modeling capability was strong.

The Pedersen-Gordon model (also referred to as the zero-limit profile model; Hall, 1982) requires that two families of modes be considered. The second family of modes, however, becomes an important consideration only at short ranges, at low frequencies, and under weak gradient conditions. In this sense, the second family plays a role similar to that of the branch-line integral associated with other branch-cut approaches. For most applications, only the first family of modes is considered. The procedure adopted at NEL during the late 1960s entailed precalculating first-family eigenvalues for selected sets of the controlling parameters. The controlling parameters are  $\rho = (g_A/g_B)^n$ , where  $g_A$  and  $g_B$  are the above-layer and below-layer velocity gradients evaluated at the top of each layer, and  $M$ , the so-called "ducting" parameter, defined as

$$M = 2\pi^{1/2}g_A^{1/2}f^{3/2}Z_L/C_s. \quad (13)$$

Thus, for a given value of  $\rho$ , the real and imaginary parts of the eigenvalues were calculated and stored for values of  $M$  ranging from 1 to 100 in steps of 0.25. Needless to say, even for only 60 modes, this procedure resulted in the storage of thousands of punched cards.

\*In contemporary literature, Airy functions are usually used instead.

Sets of eigenvalues were calculated and stored for only a few values of  $\rho$ , and predictions had to be limited to above-layer and below-layer gradients that resulted in values of  $\rho$  very close to the few stored values. The procedure for making a prediction entailed selecting stored sets of eigenvalues for values of  $M$  on either side of that value determined from input data. These stored sets were then interpolated by the transmission loss program to arrive at the correct set of eigenvalues. Since the eigenvalues are independent of source-receiver geometry, predictions could be made for several source-receiver depth combinations without having to recalculate new sets of eigenvalues. This procedure was reasonably efficient when predictions were made for a particular sonar system, i.e., a single frequency. When predictions had to be made at several frequencies, the procedure became labor intensive.

This approach may seem crude in comparison to contemporary prediction procedures. Indeed, such models as ASTRAL and RAYMODE perform all required computations "on the fly," although many liberties have been taken by the model developers in making approximations to yield relatively fast execution times. Kuperman et al. (1986) and Porter et al. (1987) are developing the Wide-area Rapid Acoustic Prediction (WRAP) system in which certain modal quantities are precalculated at selected spatial nodes in an effort to produce a high-speed three-dimensional sound field prediction capability. Thus the idea of precalculating intermediate modal quantities is still considered a viable approach in circumventing calculations that are numerically intensive.

There is strong temptation to suggest that a normal-mode model, in conjunction with precalculated sets of eigenvalues, be considered for implementation at FNOC to handle the surface-duct propagation prediction function. The large storage capacity needed to accommodate thousands of precalculated eigenvalues would not be a serious imposition for shore-based mainframes. The propagation modeling commonality requirement recently issued would necessitate that the same prediction function be implemented in on-board systems as well. Computer hardware presently being used by on-board systems precludes this possibility. The addition of an optical disk would lend credence to a precalculated approach, even for on-board systems.

This approach has considerable appeal from a strictly computational point of view. Some disadvantages, however, need to be considered. One of these disadvantages pertains to the possible inflexibility of a two-layer model. Experimental data (Anderson and Pedersen, 1976) indicate that other distinct near-surface velocity profile configurations are just as prominent as the surface duct. The modeling requirements imposed by these other profile configurations demand a more rigorous multiple-layer treatment. Rigorous solutions are not likely to be implemented

without problems. The reader interested in further details on problems that can be encountered is referred to Pedersen and McGirr (1982, pp. 97-108).

Even when a two-layer modeling approach is applicable, there are some concerns associated with the  $n^2$ -linear profile model. These concerns are discussed in the next few sections.

## 2. Sharp Discontinuity at the Layer Depth

The artificiality of the sharp discontinuity that the  $n^2$ -linear profile model imposes at the layer depth has been a source of some concern (Furry, 1946) since the model was first exploited. In many instances actual velocity profile data exhibit what appears to be a sharp discontinuity. In just as many if not more cases, the reversal in sign of the gradient is gradual. The concept of layer depth is indeed elusive. Furthermore, even when a point can be identified as the layer depth, there is a natural hesitation to proceed with sound field calculations based on the  $n^2$ -linear profile model.

Other choices of velocity profile models, complete with solutions to the reduced wave equation that are expressible in terms of well-known tabulated functions, are available. For example, the reader is referred to Murphy and Davis (1974), wherein they discuss the use of Weber functions when  $n^2(z)$  is nearly parabolic. The immediate question is, just how many such possible approaches are needed to address the set of all possible profile configurations?

There is strong incentive to give serious consideration to propagation models that provide accurate solutions for arbitrary velocity profile representations. This point is discussed briefly as a recommendation in Section V.

## 3. Departure from Linearity

The illustrations in Figure 2 indicate the depth variation in  $C(Z)$ , as well as in  $n^2(Z)$ . The variation in  $C$  is not quite linear in  $Z$ . A question of interest is, what impact does this slight departure from linearity (if linearity is indeed the proper criterion) have on various intermediate calculations that are involved in producing an estimate of the sound field? Since velocity profiles converted from in situ bathythermographs (BTs) do not necessarily exhibit a linear depth dependence, this question should be asked in reference to the shape factor associated with a given set of velocity profile data. As indicated in Appendix F, the  $n^2$ -linear model appears to be a good approximation.

## 4. Shape Factor

The previous discussion indicates that the curvature introduced by the  $n^2$ -linear profile model is negligible. Suppose that actual profile data indicate that  $C^3(Z)$  is linear in depth. Restricting attention to depths down to the layer depth, this profile model takes the form

$$C^3(Z) = C_0^3(1 + bZ), \quad (14)$$

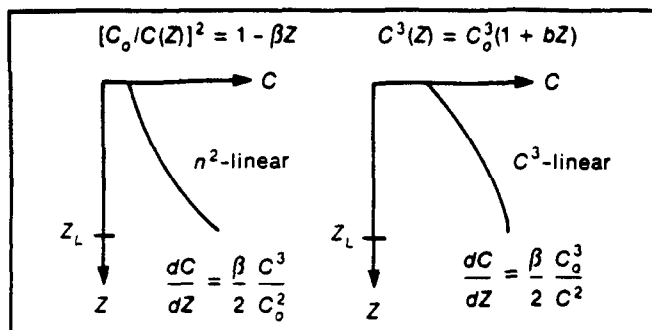


Figure 4. The  $n^2$ -linear and  $C^3$ -linear velocity profile models.

where  $b = 3g_0/C_0$  and  $g_0$  is the velocity gradient at the surface. Figure 4 illustrates both the  $n^2$ -linear and the  $C^3$ -linear profiles for comparison.

The  $C^3$ -linear profile representation is not as popular as the  $n^2$ -linear model, even though there are surface-duct environments for which it would yield a better fit. Unfortunately, the corresponding analytical solutions are not expressible in simple, closed form, as is the case for the  $n^2$ -linear model. The corresponding phase integral accedes to straightforward evaluation, and the resulting expression for the maximum number of trapped modes is (see Appendix G)

$$N = \frac{1}{4} + \frac{2}{3} (f/g_0) \sin^3 \theta_0 / \cos^2 \theta_0. \quad (15)$$

By contrast, the corresponding analysis for the  $n^2$ -linear model leads to (see McGirr, 1983)

$$N = \frac{1}{4} + \frac{2}{3} \pi^{-1} k_0 \beta^{1/2} Z_L^{3/2}. \quad (16)$$

For example, consider a 50-m layer with sound velocities of 1500 m/s at the surface and 1500.9 m/s at the bottom of the duct. For a constant-gradient profile model (i.e.,  $C$ -linear), these values yield a velocity gradient of 0.018  $\text{sec}^{-1}$ . For the  $n^2$ -linear model, the parameter  $\beta$  is  $2.4 \times 10^{-5} \text{ m}^{-1}$  and the velocity gradient as a function of depth is given by  $dC/dZ = \frac{1}{2} \beta C^3 / C_0^2$ . For the  $C^3$ -linear model, the parameter  $b$  is  $3.6 \times 10^{-5} \text{ m}^{-1}$  and the velocity gradient as a function of depth is given by  $dC/dZ = \frac{1}{2} b C_0^3 / C^2$ . The gradients evaluated at the surface and at the layer depth are summarized in tabular form as follows:

|                | $n^2$ -linear | $C^3$ -linear |
|----------------|---------------|---------------|
| at surface     | 0.0179838     | 0.0180108     |
| at layer depth | 0.0180324     | 0.0179784     |

For a frequency of 5000 Hz, the number of trapped modes is 7.942 and 7.948 for the  $C^3$ -linear and  $n^2$ -linear models, respectively. The fact that the two profile models produce the same number of modes does not necessarily imply that the resulting sound field

estimates would be the same. This agreement, along with the good agreement between  $n^2$ -linear and  $C^3$ -linear expressions for the modal cycle range (see Appendix G), suggests that the  $n^2$ -linear profile model is robust with regard to the shape-factor issue.

#### IV. Coupling of Surface Scattered Energy

The primary dissipative contributions to total surface-duct propagation loss are (1) volume absorption, (2) surface reflection loss, and (3) diffractive leakage into the negative-gradient region below the duct. Each of these losses can be added (in decibel space) to the normal-mode solution or they can be lumped together into a mode-dependent attenuation coefficient and included in the mode sum. The first two forms of loss increase with increasing frequency, whereas the third decreases. What is missing from this simple formulation is any prescription for interactive effects. A proper accounting of interaction between surface scattering and leakage entails coupling the surface-scattered energy directly into the normal-mode sum. Leakage is not the most apt description of the process, since much of the surface-scattered energy that gets into the below-layer region is by coupling between trapped and untrapped modes, as well as by leaky modes.

When surface-scattered energy is coupled into the mode sum, the resulting sound field can differ significantly from results generated by a model that includes only a surface-reflection-loss term. That is, when the scattering process is treated as a specular reflection process, there is no mechanism to simulate the propagation of surface-scattered energy into the thermocline region. For calm seas a surface-reflection-loss model can adequately account for energy lost to the scattering process. For fully developed seas, however, a considerable fraction of the energy is scattered in nonspecular directions.

These notions can be put into clearer perspective by giving some consideration to the coherent ( $I_c$ ) and incoherent or random ( $I_r$ ) components of signal intensity, that is,  $I = I_c + I_r$ . The fraction of energy in the coherent component, say  $f$ , is given by  $f = I_c / (I_c + I_r)$ . Let  $f_s$  denote the fraction of energy remaining in the coherent component after reflection from the surface and let  $f_v$  denote the fraction remaining after dissipation due to volume absorption along the path of propagation. Then the fraction of energy remaining in the coherent component arriving at the receiver, say  $f_R$ , is given by  $f_R = f_s^N f_v$ , where  $N$  is the number of surface reflections.

Signals that propagate via a surface duct are subjected to numerous encounters with the surface boundary. If the surface is perfectly smooth, i.e.,  $f_s = 1$ , then  $f_R$  is essentially just  $f_v$ . If the surface is rough, however, then  $f_s < 1$ , and for sufficient separation between source and receiver,  $f_R \rightarrow 0$ . This

condition indicates that a substantial fraction of energy propagates incoherently, or in terms of the scattering process, a significant amount of energy scatters off the surface in nonspecular directions. Thus, energy carried by low-order modes (small grazing angles for ray equivalents) can scatter off a rough surface with steeper angles. If the angles are steep enough, energy that is ordinarily trapped in the duct escapes into the below-layer region. Most mode codes do not account for incoherently scattered energy.

Under the proper conditions, then, not only can the signal coherency ( $f_R/[1 - f_R]$ ) of the trapped modes degrade, but a significant proportion of the incoherently scattered energy can leak out of the duct. For example, a shallow duct (small barrier) where both in-layer and below-layer gradients are weak (small interface reflections) and a rough sea surface (incoherent scattering) provide conditions conducive to enhanced cross-layer detection performance at the expense of in-layer performance. This circumstance conforms with the situation described in the introductory remarks.

A consideration of some importance is that boundary scattering is not an inherent feature of wave solutions. This point is often missed by casual users of propagation codes. What must be kept in mind is

that boundary reflection loss models account for the fraction of energy that scatters only in the specular direction. Bucker (1980) takes surface-scattered energy into account by adding randomly phased scattering terms to the coherent mode sum. He essentially uses ray theory in combination with mode theory to couple surface-scattered energy into the total sound field solution. The additional mode-to-ray and ray-to-mode interaction terms are incoherently summed to obtain the total intensity due to the scattered field. The scattering (or interaction) integrals developed by Bucker are presented in Appendix H.

Bucker (1980) demonstrates the theory summarized in Appendix H by comparing experimental data to calculations made both with and without the scattering integrals. The propagation loss calculations were made using a Pedersen-Gordon-type two-layer, normal-mode model. The model inputs along with the split-beam and surface-reflected rays are presented in Figure 5.

Figure 6 illustrates two propagation loss vs. range curves. The solid and dashed curves correspond, respectively, to calculations made both with and without the scattering integrals. The differences between the two curves do not become significant until the source-receiver separation range reaches about 7 kyd. Beyond this range the peaks in the multipath beat

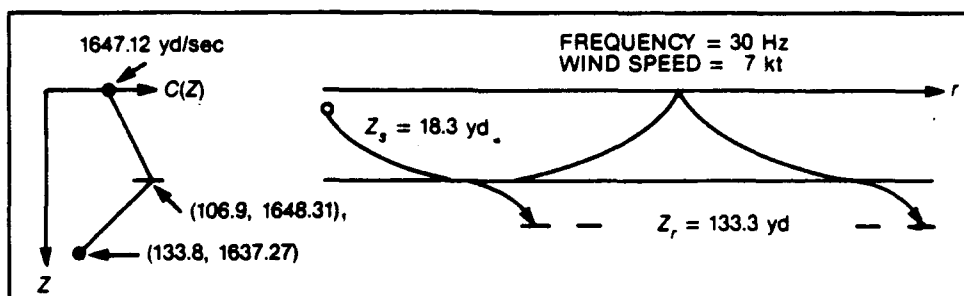


Figure 5. Model inputs and critical rays for scattering integral test case.

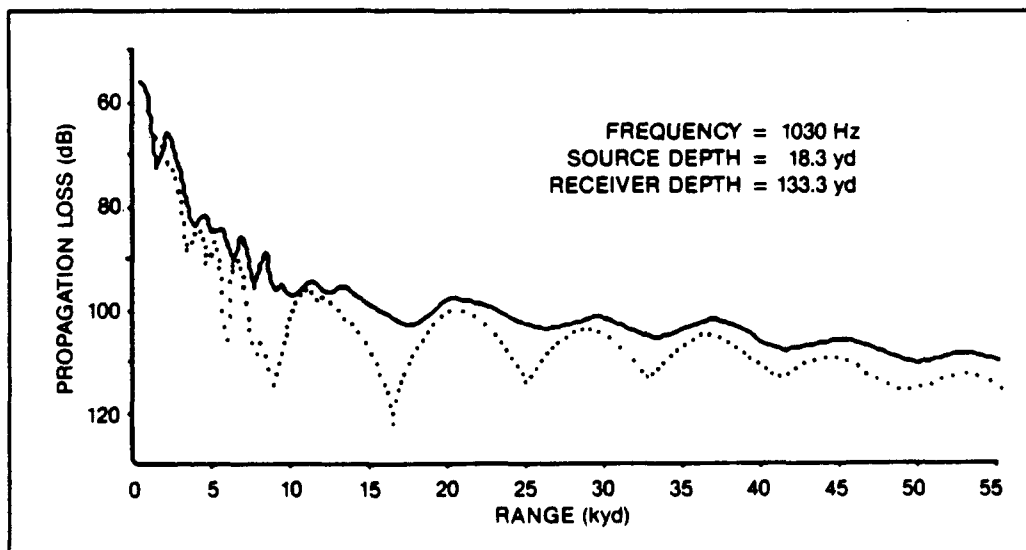


Figure 6. Propagation loss curves for cross-duct case. Solid and dotted curves correspond, respectively, to calculations made both with and without Bucker's scattering integrals.

structure are 1-2 dB more optimistic for the solid curve. The interference nulls for this curve are noticeably less extreme. This latter feature is a characteristic directly attributable to the contribution of incoherently scattered energy.

Similar comparisons for the in-layer case are not available, although Bucker (1980) notes that the differences are not as dramatic for this case. He further notes that the major differences occur in the interference nulls where incoherently scattered energy tends to fill in the sound field.

The interpretation of these results with regard to the main issue—anomalous SHARPS-generated surface-duct predictions—is that even though calculations based on the scattering integrals yield more realistic cross-layer predictions, the contribution of incoherently scattered energy is not significant enough to explain the anomalous cross-layer detection ranges, as reported in the message traffic received by FNOC. Indeed, the differences between in-layer and cross-layer predictions reported by Bucker (1980) are on the order of 2 or 3 dB—as determined from the interference peaks—for ranges beyond about 10 kyd. Thus, there appears to be no basis to support the anomalous cross-layer detection ranges as purportedly predicted by SHARPS.

## V. Computational Artifacts

A problem that is difficult to overcome when using hybrid solutions is the appearance of discontinuities that typically occur as the method of solution switches from one method to another. If the decision tree that determines the method of solution is properly designed and correctly implemented, the magnitude of the jump discontinuities should be almost negligible. In Active RAYMODE the switch from the normal-mode summation method to one of the special integration methods occurs when the number of modes for a given  $k$ -segment (or duct) exceeds 10.

To get an idea of how serious this problem is with the Active RAYMODE model, consider the following example. The velocity profile is illustrated in Figure 7. The main interest here is in the surface-duct portion of the propagation channel. Hence, the lower part of the profile consists of negative gradients from the layer depth down to a high-loss bottom at a depth of 1000 m. Both source and receiver are in the surface duct at depths of 6 m and 18 m, respectively. A zero wind speed was selected to discourage contributions from the surface loss model. Similarly, a high-loss bottom was specified to diminish contributions from bottom-reflected paths.

Active RAYMODE was executed at several frequencies in the neighborhood of 2300 Hz to expose any discontinuity that might arise as a consequence of using distinct methods of calculation. At this frequency the

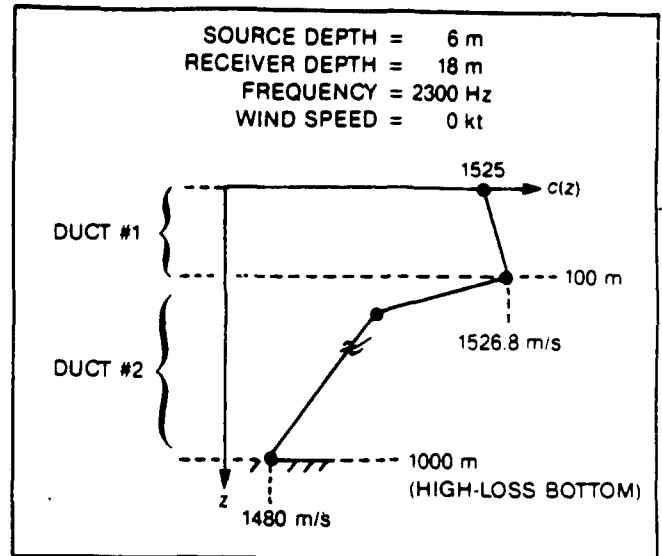


Figure 7. Inputs for discontinuity test case.

number of modes should just exceed 10. That is, with  $C_o = 1525 \text{ m/s}$ ,  $g_o = 0.018 \text{ s}^{-1}$ , and  $Z_L = 100 \text{ m}$ , the frequency corresponding to  $N$  modes is given by (see Appendix G)

$$f \cong 235.4 (N - \frac{1}{2}), \quad (17)$$

which for  $N = 10$  gives  $f = 2295.2 \text{ Hz}$ . Thus, there should be a discontinuity at some frequency in the vicinity of 2300 Hz. The scheme used in RAYMODE to determine the number of modes trapped in a duct is somewhat unorthodox (as discussed in Davis and Council, 1985b), so isolating the particular frequency at which the switch occurs from the mode-sum method to one of the integration methods requires a trial-and-error search. A few runs at several frequencies in the vicinity of 2300 Hz revealed that the expected jump actually occurs at a frequency between 2249 Hz and 2250 Hz. The discontinuity is illustrated in Figure 8, where incoherent transmission loss (TL) is plotted against frequency at a range of 5 kyd. The data shown are for frequencies varying from 2200 Hz to 2300 Hz in 10-Hz steps, except for frequencies between 2240 Hz and 2260 Hz where the step size has been cut down to 1 Hz. There is a jump discontinuity of about 2 dB between 2249 Hz and 2250 Hz.

The impact of switching from one computational method to another is just as evident when transmission loss vs. range curves are examined over a band of frequencies on either side of the switching frequency. Figure 9 presents a plot of two incoherently summed TL vs. range curves\* for frequencies within a 50-Hz neighborhood on either side of the break frequency.

\*Coherently summed TL is not offered as an option in Active RAYMODE.

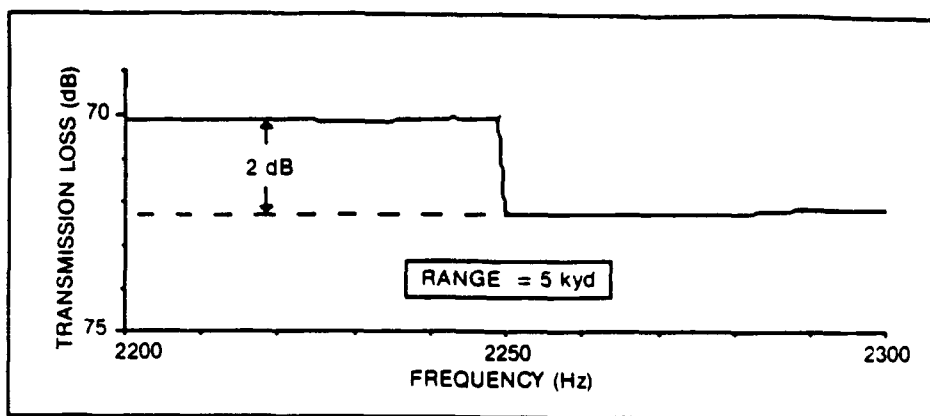


Figure 8. Discontinuity caused by switching from the mode summation method to the original RAYMODE integration method.

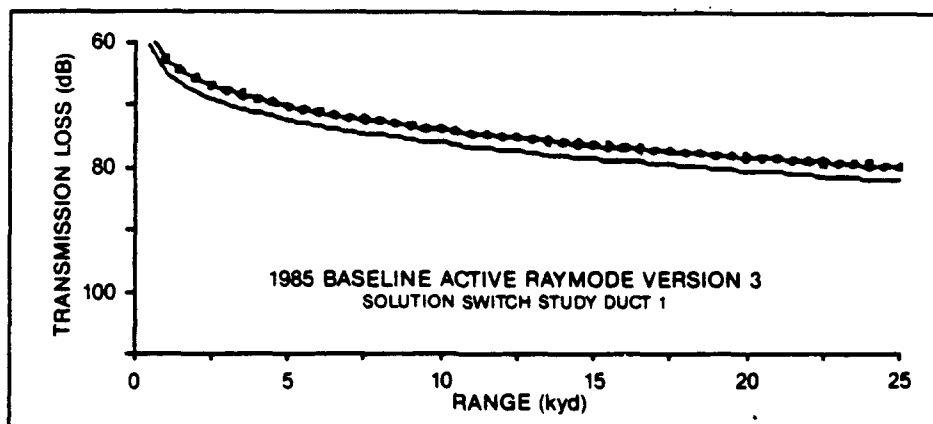


Figure 9. Transmission loss vs. range curves generated by Active RAYMODE for the frequency band less than 2249 Hz (symbols) and for the frequency band greater than 2250 Hz (solid).

According to the documented decision tree (summarized in Section II), another discontinuity is likely to occur for some frequency between 2250 Hz and 3000 Hz where there is another switch from the original RAYMODE integration (ORI) method to the special HFI method. The only circumstance for which this switch does not take place is when the method of solution switches directly from the mode-sum method to the HFI method. A brief search for the ORI  $\rightarrow$  HFI switch revealed that the switch occurs at 2752 Hz. This discontinuity is illustrated in Figure 10. Here again the jump discontinuity is on the order of 2 dB.

The discontinuity due to switching from the mode-sum method to the ORI method also yields a sudden jump for slight changes in layer depth. That is,  $z_L$ , corresponding to  $N$  modes, is given by

$$z_L = \left[ \frac{1}{4} \frac{(N - 1/4)}{\sqrt{2g_o} f} \right]^{2/3} C_o. \quad (18)$$

Substituting the values given for  $c_o$  and  $g_o$  and setting  $f = 2249$  Hz gives, approximately,

$$z_L \cong (N - 1/4)^{2/3}, \quad (19)$$

which for  $N = 10$  yields  $z_L \cong 100$  m. Thus, there should be a discontinuity observed for some layer depth in the vicinity of 100 m. An examination of this particular type of discontinuity is not pursued here, since it is of the same origin as the frequency discontinuity illustrated in Figure 8.

The size of jump discontinuities of this sort may not be of devastating significance for many cases of interest. A cause of concern, however, is that occasions can arise when a mere 2 dB can make the difference between detection and nondetection. Note that the slopes in the curves of Figure 9 are not particularly steep for ranges greater than about 5 kyd. A simple (one-way) figure-of-merit (FOM) analysis reveals that for an 80-dB FOM the low-frequency curve indicates a detection range of about 25 kyd, whereas the high-frequency curve indicates that detections can be expected to cease for ranges greater than about 18 kyd. There are probably scenarios (both active and passive) for which a discrepancy of 7 kyd can make a difference.

## VI. Summary Remarks

The surface-duct propagation loss prediction capability of the Active and Passive RAYMODE

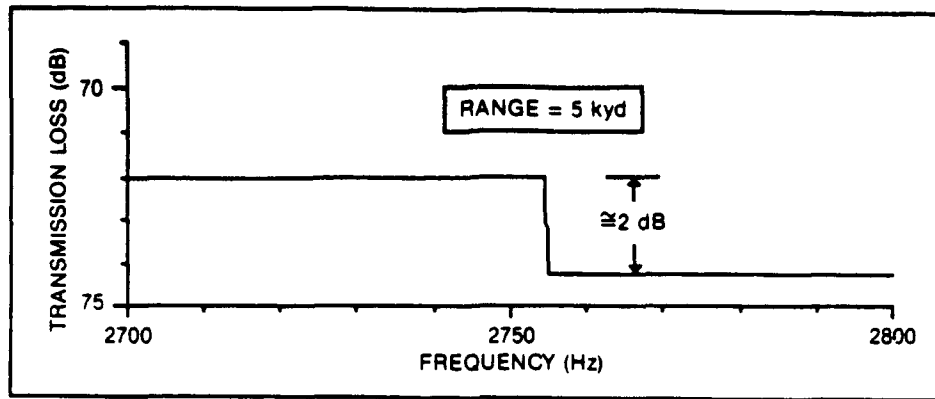


Figure 10. Discontinuity caused by switching from the ORI method to the HFI method.

models has been qualitatively assessed. This review was motivated by reports (Naval Messages) of questionable in-layer and cross-layer target detection ranges predicted by SHARPS under certain well-ducted propagation conditions. Reports of this sort are expected no matter what model is used. The largest variations in sound-velocity gradients are observed in the upper portion of the velocity profile; therefore, detection range prediction errors are expected to be greater for near-surface propagation paths.

### A. Conclusions

The review of RAYMODE model physics, (Section II and attendant appendices), reveals that calculations pertaining to surface-duct conditions can be performed by one or more methods. Each of the RAYMODE wave-field integrals can take the form of an approximate normal-mode expansion or a generalized WKB multipath expansion. If the number of propagating modes is less than 10, the dominant method is an approximate normal-mode sum. The approximations that lead to the RAYMODE normal-mode sum render the approach essentially useless for surface-duct calculations. The first approximation made is in the expression for the Wronskian, where standard WKB forms are used in place of the generalized WKB amplitude functions. The error introduced by this particular approximation, however, should be negligible for most cases except, perhaps, for surface ducts. The next approximation made is in assuming real eigenvalues. To properly apply mode theory to surface ducts, the inclusion of modal attenuation, due mainly to the ratio of in-layer to below-layer velocity gradients, is crucial.

When the RAYMODE wave-field integrals are evaluated using generalized WKB expansions, there are three distinct algorithms from which one is selected according to a decision tree (see Section II). Each of these algorithms solves an integral of Fourier type. Two of these methods, the ORI method, and the HFI method, are reviewed herein. Although stationary-phase (saddle-point) procedures are applied in both of these methods, in neither case is the stationary-phase

formula relied upon. Instead, the integrals are evaluated over a restricted domain using asymptotic expansions. Moreover, the HFI method includes a special algorithm for the evaluation of a field point in the vicinity of a caustic. The decision rule encompasses the approximate normal-mode sum as well; thus, the RAYMODE decision process effectively partitions the wave-number integration into low- and high-frequency components. Since this partitioning is accomplished for a given duct, there is always the possibility that several of the RAYMODE methods are exercised during a single model execution.

The magnitude of error that might be introduced by the ORI and the HFI methods is difficult to assess in general. The accuracy of these methods is closely associated with the validity of WKB solutions to the depth-separated wave equation. The local sound field is well approximated by WKB solutions for certain depth intervals referred to as "allowed" regions. These methods may be inaccurate in complementary intervals, referred to as "forbidden" regions. In an attempt to improve standard WKB solutions, the model developer uses a generalized WKB solution, which tends to degenerate to the standard WKB form only when the field point is far removed from a turning point. The generalized WKB amplitude functions are determined iteratively. The only other instance when the standard WKB form is relied upon, is in arriving at an approximate expression for the Wronskian. This approximation impacts all of the RAYMODE methods reviewed herein. A previous RAYMODE evaluation conducted by Bartberger (1981) indicates that the error introduced by the special integration methods has its major impact on coherently summed results, being somewhat mitigated when the results are incoherently summed. The general requirements justifying a stationary-phase analysis are probably not met at low frequencies, i.e., phase oscillations may not be rapid enough to effect the required cancellations. As far as the "extension" of this method to include those cases when the point of stationary phase falls outside the

limits of integration is concerned, the procedure used in RAYMODE appears to have been chosen out of convenience, i.e., so that the Fresnel integral algorithms can be used. The specific steps taken by the model developer in applying stationary-phase methods are not universally accepted as being the most effective (see Weinberg, 1981).

The surface reflection loss submodel is reviewed in Section II. An estimate of surface loss (SL) is determined from the sum of two independent terms,  $SL_1$  and  $SL_2$ . The evaluation by Keenan (1983) of the SUBCOM surface loss model (the one used in RAYMODE) shows that the  $SL_1$  term represents incoherently scattered energy characteristic of a Kirchhoff solution. Keenan further notes that this term is dominant for frequencies below about 1 kHz. Since incoherent scattering should dominate the solution only for large values of the Rayleigh parameter, Keenan concludes that the  $SL_1$  term is not intuitively satisfactory as an estimator of rough surface loss.

The  $SL_2$  term has no angle dependence, and it is probably supposed to represent the coherent component of energy scattered at an average angle characteristic of surface-duct and convergence zone paths. Speculation of this sort is interesting, although not particularly productive. Until the model developer subjects his derivation to peer review, however, any critique of the model physics amounts to little more than speculation. Results generated by this model were evaluated, along with results generated by several other surface loss models. Comparisons are included in a report that presents the findings and recommendations of a surface loss model working group (Eller, 1984). Interestingly, the surface loss model recommended by this working group has not been adopted.

A special surface-duct leakage routine, included in a previous version of Passive RAYMODE, is conspicuously missing from the present version. A review of the corresponding computer code reveals at least one error, along with expressions that bear a curious resemblance to those normally associated with WKB phase integral methods. Corrections could be made quite readily, although suggestions offering more promise are made in the recommendations section.

Before a two-layer surface-duct submodel is decided upon, serious consideration should be given to the consequences: namely, its inflexibility with regard, not only to velocity profile fit, but to its inability to address more general near-surface profile configurations. If such a submodel is selected, there are ways to improve computational efficiency (see Section III).

The omission of any means to couple surface-scattered energy into the sound field is not a deficiency peculiar to the RAYMODE codes. Indeed, few models address this important feature. For the example discussed in Section IV, the inclusion of Bucker's scattering integrals can bring the interference peaks up

(reduce the loss) by 2 dB for the longer ranges. Just as importantly, the interference nulls tend to get washed out. For detection range calculations based on coherent signal-to-noise ratios, the contribution of incoherently scattered energy would be significant, but only if the correct statistical distributions are considered (as discussed in Pedersen and McGirr, 1983). If only averaged signal-to-noise ratios are considered, the significance is less dramatic. Consideration should be given to including the scattering integrals, since their omission can yield slightly pessimistic cross-layer predictions.

Discontinuities that occur when the method of solution switches from one form to another appear to be on the order of a couple of decibels, at least as determined by the brief assessment presented herein. Numerical artifacts of this sort fall into the category of nuisances and are typical of hybrid methods. To the extent that the size of these discontinuities does not exceed about 2 dB, they are not considered to be major deficiencies.

In any case, none of the Active RAYMODE model deficiencies discussed herein is likely to cause anomalous cross-layer detection ranges, such as those purportedly predicted by SHARPS. The very appearance of anomalous surface-duct detection ranges generated by SHARPS naturally raises the question, what set of surface-duct conditions could possibly produce greater detection ranges for cross-layer geometries than for in-layer geometries? For a well-defined classic surface duct, an answer is not immediately forthcoming. If care is not taken in identifying—acoustically—what does or does not constitute a well-defined surface duct, then interpretations of the resulting acoustic predictions are more-or-less at the mercy of possibly invalid interpretations of the controlling velocity profile. This latter possibility essentially reflects the essence of the so-called sonic-layer-depth (SLD) problem.

As a case in point, consider the following example. Suppose the input velocity profile (as generated by a pre-SHARPS program) takes the form illustrated in Figure 11. The near-surface portion of this profile consists of an isovelocity duct overlaying a weak gradient layer. Even though the SLD for this case would be reported in the SHARPS message as 50 m, the first two layers actually comprise the in-layer portion of a weak surface duct. The difference in the velocity gradients of these two layers is acoustically negligible. The major gradient discontinuity occurs between the second and third layers; therefore, the bottom of the in-layer portion of the near-surface channel actually corresponds to 150 m.

For demonstration, however, let the upper two layers be arbitrarily identified as the in-layer and below-layer components of the surface duct, which would be the logical interpretation formulated by a recipient of a

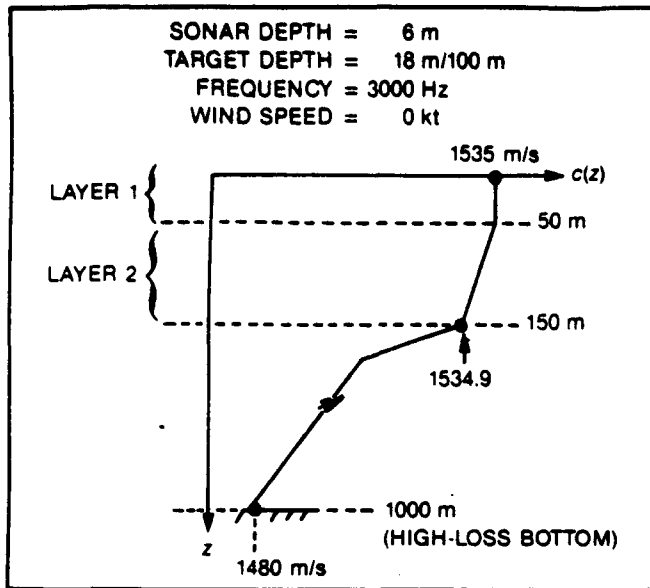


Figure 11. Sound velocity profile for an SLD test case.

SHARPS message claiming a 50-m SLD. Let the sonar and target depths be 6 m and 18 m, respectively, for the "in-layer" case, and 6 m and 100 m, respectively, for the "cross-layer" case. Figure 12 presents (a) in-layer and (b) cross-layer propagation loss vs. range curves for a frequency of 3000 Hz. Not surprisingly, the cross-layer curve is more optimistic than the in-layer curve. By virtue of their weak gradients, the first two layers of this profile do not constitute a well-defined surface duct, but because of the way SLD is defined, curves (a) and (b) of Figure 12 would be interpreted as predictions for in-layer and cross-layer geometries.

## B. Recommendations

The most important deficiency in the RAYMODE codes that needs to be rectified is the omission of any means to account for interduct coupling. This problem, in general, is not easily corrected without recourse to rigorous normal-mode theory; even then, numerical problems can arise during attempts to find eigenvalues in interduct situations. The easiest solution is to add a special surface-duct module, and simply ignore other interduct coupling problems. One possibility is to resurrect the surface-duct submodel from a previous version of Passive RAYMODE. A brief discussion of this submodel is presented in the document of Davis and Council (1985b), as well as in Section II. Some additional work on this submodel is indicated. ASTRAL\* already has such a module (Ryan, 1980; White, 1988); therefore, it could be incorporated rather easily into the RAYMODE codes. Inasmuch as

\*ASTRAL: ASEPS' Transmission Loss (Spofford, 1979)  
 ASEPS: Automated Signal Excess Prediction System

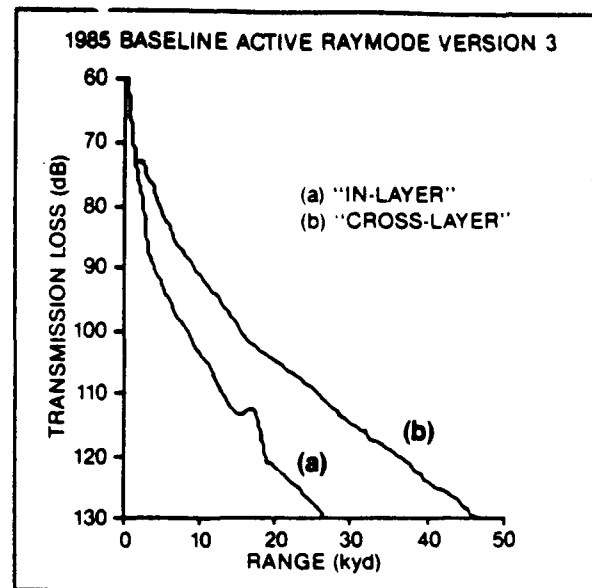


Figure 12. Transmission loss curves for an SLD test case.

ASTRAL is one of the standard range-dependent propagation loss models, this approach would automatically satisfy the OPNAV commonality requirement.

The ASTRAL surface-duct module does not deal with energy that is incoherently scattered by the surface. To properly address surface-scattered energy, this module would have to be upgraded. The incorporation of Bucker's (1980) scattering integrals is easy conceptually, but could be costly. Actually there are three costs to consider: (1) the cost of implementation, and once implemented, the costs in (2) storage and in (3) run-time that would be incurred operationally.

Instead of using a two-layer surface-duct model, serious consideration should be given to using a normal-mode model that can handle up to, say, five layers. In this way, accurate predictions can be made for all important near-surface velocity profile configurations. The major objections to this approach naturally pertain to excessive run-time and storage requirements, but the rate of advances presently being made in computer technology suggests that these requirements are achievable in the very near future for both ashore and afloat systems. Moreover, as available computing resources become more powerful, the emphasis in modeling upgrades should focus on improving the quality of predictions vice quantity.

This recommendation is not entirely new (McGirr, 1983) although a full-wave treatment is recommended instead of an approximate approach based on WKB phase-integral methods. Consider the expression that gives the (far-field) acoustic pressure for a receiver at depth  $z$  and range  $r$ , i.e.,

$$p(r,z) = C \sum_n u_n(z_0) u_n(z) \exp(ik_n r) / (k_n r)^{1/2}. \quad (20)$$

where  $z_o$  is the source depth, and the  $u_n$  are normalized modal depth functions. The  $k_n$  (eigenvalues) are functions of frequency and the environmental-acoustic input profile (velocity profile, bottom depth, bottom loss, and surface loss), but they are independent of source depth and receiver depth. The  $u_n(z)$  are functions of the  $k_n$ . Thus, there is a natural hierarchical ordering of the required computations for any given run.

Suppose that predictions are required for a single source depth and three receiver depths at some frequency, say,  $f_o$ , for which there are  $N$  modes. First the  $N$  eigenvalues are determined and stored. Then, the depth functions  $\{u_n(z_o)\}$  are computed and stored. Then, three sets of  $N$  depth functions  $\{u_n(z_j)\}$ ,  $j = 1, 2$  and  $3$ , are computed and stored. For each receiver depth ( $z_j$ ), a transmission loss vs. range curve can be determined from

$$TL = 10 \log |pp^*| \quad (21)$$

where, for long ranges, the normalized acoustic pressure is given by

$$p = \sum A_n u_n(z) \exp(ik_n r) / \sqrt{r}, \quad (22)$$

and where  $A_n = C u_n(z_o) / k_n$ . The expression for  $p$  has been put into this form to emphasize that the  $A_n$  are simply retrieved from storage during this stage of computation. The number of terms in the sum is actually a function of range. That is, modal attenuation increases with range, therefore, fewer terms are needed as range increases. A relatively conservative criterion used in determining when to stop the summation entails comparing the last four terms to the cumulative sum. If the relative contribution is less than 0.0001, then the summation is stopped.

The computational strategy described above can be exploited even more aggressively in the design of prediction systems dedicated to the generation of data in support of predeployment acoustic assessments. Assessments of this sort are typically based on archived data. Standard Navy data bases could be expanded to include precalculated intermediate modal quantities tailored to specific system parameters and most-probable target depths. This procedure is similar to the one discussed in Section II. To incorporate updated oceanographic data, however, would require adding a perturbation scheme, or, using a prediction system such as WRAP, which is presently under development by Kuperman et al. (1986) and Porter et al. (1987).

Finally, insofar as anomalous SHARPS-generated, cross-layer detection ranges are concerned, this circumstance is more than likely a consequence of the long-standing SLD problem, as mentioned in the introduction and discussed in the conclusions. This problem

is also discussed by McGirr (1983) and by Renner and Kirby (1983). Since the anomalous SHARPS predictions are in contrast with those generated by shipboard prediction systems, (the latter results are purportedly the more reasonable) the OPNAV imposed commonality requirement needs to be extended to include any and all peripheral software and data bases that can impact predictions generated by standard acoustic models. Thus, as a final recommendation, the organization responsible for configuration control of Fleet acoustic prediction systems should ensure that all such software packages and data bases essentially produce identical results. For the case at hand, this action entails replacing the BT-conversion software presently used at FNOC with the appropriate software that is used by (standard) shipboard prediction systems.

## VII. References

- Anderson, E. R. and M. A. Pedersen (1976). *Surface-Duct Sonar Measurements* (SUDS I - 1972). Technical Report, Naval Undersea Center, San Diego, CA, NUC TP 463.
- Barnard, G. R. and Deavenport, R. L. (1978). Propagation of sound in underwater surface channels with rough boundaries. *J. Acoust. Soc. Am.* 63:709-714.
- Bartberger, C. L. (1981). *An Investigation of the Physics of the RAYMODE Model*. Naval Air Development Center, Warminster, PA, NADC Report 82009-30.
- Beckmann, P. and A. Spizzichino (1963). *The Scattering of Electromagnetic Waves from Rough Surfaces*. Macmillan, New York.
- Bleistein, N. and R. A. Handelsman (1986). *Asymptotic Expansions of Integrals*. Dover, New York.
- Brekhovskikh, L. M. (1980). *Waves in Layered Media*. Academic Press, Inc., New York, 2nd edition.
- Brekhovskikh, L. M. and Yu. Lysanov (1982). *Fundamentals of Ocean Acoustics*. Springer-Verlag, New York.
- Bucker, H. P. (1970). Sound propagation in a channel with lossy boundaries. *J. Acoust. Soc. Am.* 48:1187-1194.
- Bucker, H. P. (1980). Wave propagation in a duct with boundary scattering (with application to a surface duct). *J. Acoust. Soc. Am.* 68:1768-1772.
- Cox, C. S. and W. H. Munk (1954). Measurement of the roughness of the sea surface from photographs of the sun glitter. *J. Optic. Soc. Am.* 44:838-850.
- Davis, J. A. and O. P. Council (1985a). *ACTIVE RAYMODE*. Planning Systems Inc., McLean, VA, PSI TR-S310045.
- Davis, J. A. and O. P. Council (1985b). *PASSIVE RAYMODE*. Planning Systems Inc., McLean, VA, PSI TR-S310046.

- Deavenport, R. L. (1978). *RAYMODE Physics Evaluation*. Naval Undersea Systems Center, New London, CT, Encl(2) to NUSC/NL ltr ser 9312-55.
- DiNapoli, F. R. and Deavenport, R. L. (1979). Numerical Models of Underwater Acoustic Propagation. In *Ocean Acoustics*, Chap. 3, by J. A. DeSanto (ed.), Springer-Verlag, New York.
- Eller, A. (1984). *Findings and Recommendations of the Surface Loss Model Working Group: Final Report*. Naval Ocean Research and Development Activity, Stennis Space Center, MS, NORDA TN 279.
- Erdlyi, A. (1956). *Asymptotic Expansions*. Dover, New York.
- Freehafer, J. E. (1951). Phase-integral Methods, and The Field Integral, (Sect 2.10). In *Propagation of Short Radio Waves*, D.E. Kerr (ed.), McGraw-Hill, New York, sect. 2.8 and 2.10.
- Furry, W. H. (1945). *Methods of Calculating Characteristic Values for Bilinear M Curves*. Massachusetts Institute of Technology, Boston, MA, MIT Laboratory Report 680.
- Furry, W. H. (1946). *Theory of Characteristic Functions in Problems of Anomalous Propagation*. Massachusetts Institute of Technology, Boston, MA, MIT Laboratory Report 795.
- Gordon, D. F. and H. P. Bucker (1984). *Arctic Acoustic Propagation Model with Ice Scattering*, Naval Ocean Systems Center, San Diego, CA, NOSC TR 985.
- Hall, M. (1976). Mode theory of wave propagation in a bilinear medium: The WKB approximation. *J. Acoust. Soc. Am.* 60:810-814.
- Hall, M. (1982). Normal mode theory: The role of the branch-line integral in Pedersen-Gordon type models. *J. Acoust. Soc. Am.* 72:1978-1988.
- Harvard University Computation Laboratory (1945). *Tables of the Modified Hankel Functions of Order One-Third and of Their Derivatives, Vol. II*. Harvard University Press, Cambridge, MA.
- Houston, R. A. (1915). *A Treatise on Light*. Longmans, Green & Co., New York.
- Keenan, R. E. (1983). *Final Report Volume IV: SUBCOM, FAME, RAYMODE and FACT Comparisons of Accuracy and Computation Time in a Surface Duct Environment*. Science Applications Inc., McLean, VA, SAI-84-153-WA.
- Kibblewhite, A. C. and R. N. Denham (1965). Experiment on propagation in a surface sound channel. *J. Acoust. Soc. Am.* 38:63-71.
- Kirby, W. D. (1982). *Technical Description for the Ship Helicopter Acoustic Range Prediction System (SHARPS III)*. Science Applications Inc., McLean, VA, SAI-83-1071.
- Kuperman, W. A., M. B. Porter, F. Ingenito and S. A. Piacsek (1986). Wide-area Rapid Ocean/Acoustic Prediction. In *Proceedings of the Ocean Prediction Workshop*, Institute of Naval Oceanography, Stennis Space Center, MS.
- Leibiger, G. A. (1968). *Application of Normal Mode Theory to Propagation of 3.5 kHz Pulses in Shallow Water*. Vitro Laboratories, VL-2476-9-O.
- Leibiger, G. A. (1971). *A Combined Ray Theory-Normal Mode Approach to Long Range, Low Frequency Propagation Loss Prediction*. Naval Underwater Sound Center, New London, CT, NUSC Technical Memorandum PA3-0109-71.
- Marsh, H. W. (1950). *Theory of Anomalous Propagation of Acoustic Waves in the Ocean*. U.S.N. Underwater Sound Laboratory, New London, CT, USNUSL Report 111.
- Marsh, H. W. and M. Schulkin (1962). *Underwater Sound Transmission*. AVCO Marine Electronics Office (unpublished technical memorandum).
- McGirr, R. W. (1983). *Comments and Issues Pertinent to SHARPS III Near-surface Propagation Modeling*. Naval Ocean Research and Development Activity, Stennis Space Center, MS, NORDA Report 64.
- McGirr, R. W., L. K. Arndt and E. D. Chaika (1972). *Fast NISSM, A Utility Version of the Navy Interim Surface Ship Sonar Prediction Model*. Naval Undersea Research and Development Center, San Diego, CA, NUC TP-309.
- Murphy, E. L. and J. A. Davis (1974). Modified ray theory for bounded media. *J. Acoust. Soc. Am.* 56:1747-1760.
- Pedersen, M. A. and D. F. Gordon (1965). Normal mode theory applied to short-range propagation in an underwater acoustic surface duct. *J. Acoust. Soc. Am.* 37:105-118.
- Pedersen, M. A. and R. W. McGirr (1982). *Use of Theoretical Controls in Underwater Acoustic Model Evaluation*. Naval Ocean Systems Center, San Diego, CA, NOSC TR 758.
- Pedersen, M. A. and R. W. McGirr (1983). *Experimental and Theoretical Statistical Distributions of Underwater Acoustic Propagation Losses*. Presented at the 11th International Congress of Acoustics, Paris, Paper 28-11
- Porter, M. B., W. A. Kuperman, F. Ingenito and A. A. Piacsek (1987). Rapid computation of acoustic fields in three-dimensional ocean environments. *J. Acoust. Soc. Am.* 81(SI):S9.
- Renner, W. W. and W. D. Kirby (1983). *Sound Velocity Profile Filter Evaluation*. Science Applications, Inc., McLean, VA, SAI-84-227-WA.
- Ryan, F. J. (1980). *Virtual Mode Surface Duct Model for FACT*. Science Applications Inc., McLean, VA, SAI-81-259-WA.
- Smith, P. W., Jr. (1974). Averaged sound transmission in range-dependent channels. *J. Acoust. Soc. Am.* 55:1197-1204.

Spofford, C. W. (1979). *The ASTRAL Model, Volume I: Technical Description*. Science Applications, Inc., McLean, VA, SAI-79-742-WA.

Watson, W. H. and R. W. McGirr (1966). *A Surface Channel Propagation Loss Model I*. U.S. Navy Electronics Laboratory, San Diego, CA, NEL TM 921.

Watson, W. H. and R. W. McGirr (1972). *An Active Sonar Performance Prediction Model*. Naval Undersea Research and Development Center, San Diego, CA, NUC TP 286.

Weinberg, Henry (1973). *Navy Interim Surface Ship Model (NISSM) II*. Naval Undersea Systems Center, New London, CT, NUSC TR 4527.

Weinberg, Henry (1981). Effective range derivative for acoustic propagation loss in a horizontally stratified ocean. *J. Acoust. Soc. Am.* 70:1736-1742.

White, DeWayne (1988). *ASTRAL 2.2: Technical Description*. Science Applications International Corporation, La Jolla, CA (draft documentation).

**Appendix A**  
**Normal-mode and Multipath Expansion Forms**

---

The review presented herein focuses on those methods that are most apt to have some bearing on surface duct propagation loss predictions. Since the propagation model used in Active RAYMODE is essentially a subset of Passive RAYMODE, most of the discussion presented in the following paragraphs serves as a review of those methods used in Passive RAYMODE that can impact predictions for surface duct environments. Indeed, at the outset of this task, the hypothesis was formulated that the special surface duct treatment found in a previous version of Passive RAYMODE can be used, with corrections and suitable modifications, to couple the surface scattered field into the mode sum, thereby yielding better sound field estimates for both in-layer and cross-layer geometries.

Passive RAYMODE is an interesting model because of the several methods that are applied to the problem of solving the wave equation. Not all of these methods are applicable to the surface duct problem of interest here, and hence attention focuses on those methods that potentially have some bearing on the problem at hand. A convenient starting point for this review is the wave equation, which, under the assumption of azimuthal symmetry and range-invariant horizontal stratification of the water column, can be expressed as

$$\frac{1}{r} \frac{\partial}{\partial r} \left( r \frac{\partial \psi}{\partial r} \right) + \frac{\partial^2 \psi}{\partial z^2} = \frac{1}{c^2} \frac{\partial^2 \psi}{\partial t^2}, \quad (\text{A1})$$

where  $r$  is range,  $z$  is depth,  $t$  is travel time,  $c$  is the velocity of sound treated as a function of depth only, and  $\psi$  is the velocity potential. Assuming a point harmonic source with  $\exp(i\omega t)$  time dependence, the velocity potential can be expressed as

$$\psi = e^{i\omega t} \Phi(r, z), \quad (\text{A2})$$

where  $i = \sqrt{-1}$ ,  $\omega = 2\pi f$ , and  $\Phi$  is a potential function dependent on the spatial variables  $r$  and  $z$ . Substitution of Eq. (A2) into Eq. (A1) yields

$$\frac{1}{r} \frac{\partial}{\partial r} \left( r \frac{\partial \Phi}{\partial r} \right) + \frac{\partial^2 \Phi}{\partial z^2} = \frac{\omega^2}{c^2} \Phi, \quad (\text{A3})$$

Since surface duct propagation is the main focus of this report, there is no need to include effects due to variations in density, and hence the density can be taken as constant (i.e.,  $\rho \equiv 1$ ). Thus, the acoustic pressure  $p$  is simply

$$p = i\omega\Phi. \quad (\text{A4})$$

Expressing  $\Phi(r,z)$  as the product of  $R(r)$ , a function of range only, and  $Z(z)$ , a function of depth only, leads to the following pair of equations

$$r^2 \frac{d^2 R}{dr^2} + r \frac{dR}{dr} + k^2 r^2 R = 0, \quad (\text{A5})$$

and

$$\frac{\partial^2 Z}{\partial z^2} + \left( \frac{\omega^2}{c^2} - k^2 \right) Z = 0, \quad (\text{A6})$$

where  $k$  is the horizontal wave number. Eq. (A5) is recognized as a form of Bessel's equation which has the solution

$$R(r) = J_0(kr), \quad (\text{A7})$$

where  $J_0(kr)$  is the zero-order Bessel function of the first kind. The usual practice in dealing with underwater sound problems is to consider the Fourier-Bessel transform, that is

$$\Phi = \int_0^{\infty} G(z_r, z_s, k) H_0^{(1)}(kr) k dk + \int_0^{\infty} G(z_r, z_s, k) H_0^{(2)}(kr) k dk, \quad (\text{A8})$$

where  $J_0(kr)$  has been replaced by the zero-order Hankel functions of the first and second kind through the relation

$$J_0(kr) = 1/2 [H_0^{(1)}(kr) + H_0^{(2)}(kr)]. \quad (\text{A9})$$

Since  $H_0^{(1)}(kr) = -H_0^{(2)}(-kr)$ , Eq. (A8) can be expressed in the form

$$\Phi = \int_{-\infty}^{\infty} G(z_r, z_s, k) H_0^{(2)}(kr) k dk \quad (\text{A10})$$

where  $G(z_r, z_s; k)$  is referred to as the depth-dependent Green's function.

The development from this point follows that of Davis and Council (1985b), although some liberties have been taken in making slight modifications in notation. Let  $U(z, k)$  and  $V(z, k)$  be linearly independent solutions of Eq. (A6), where  $U$  satisfies the upper boundary condition and  $V$  satisfies the lower boundary condition. Denoting source depth by  $z_s$  and receiver depth by  $z_r$ , the Green's function takes the form

$$G = U(z_s, k) V(z_r, k) / W, \text{ if } z_r > z_s, \quad (\text{A11})$$

or

$$G = U(z_r, k) V(z_s, k) / W, \text{ if } z_r < z_s, \quad (\text{A12})$$

where  $W$ , the Wronskian, is given by

$$W = U \, dV/dz - dU/dz \, V. \quad (\text{A13})$$

At this stage the approach used in RAYMODE is to assume that  $U$  and  $V$  can be expressed in terms of generalized WKB solutions that take the forms

$$U = u(z) \exp[i\phi(z_u, z_s)] + R_u u^*(z) \exp[-i\phi(z_u, z_s)] \quad (\text{A14})$$

for  $z_u < z_s$ , and

$$V = v(z) \exp[-i\phi(z_l, z_r)] + R_l v^*(z) \exp[i\phi(z_l, z_r)] \quad (\text{A15})$$

for  $z_r < z_l$ . A tacit assumption made in these expressions is that  $z_s < z_r$ , although there is no loss of generality since their roles can be reversed by a simple interchange of subscripts.  $R_u$  and  $R_l$  are reflection coefficients that must satisfy certain conditions at the upper and lower boundaries or turning points, respectively. In an attempt to improve upon standard WKB solutions, the amplitude functions,  $u(z)$  and  $v(z)$ , are determined iteratively.

---

†For more details see Sect. 47 of Brekhovskikh (1980)

The function appearing in the exponents is given by

$$\phi(z_1, z_2) = \int_{z_1}^{z_2} Q(z, k) dz, \quad (\text{A16})$$

where

$$Q^2(z, k) = [\omega/c(z)]^2 - k^2. \quad (\text{A17})$$

The upper and lower turning points occur at depths  $z_u$  and  $z_l$  where the function  $Q$  vanishes.

The Wronskian that appears in the denominators of Eqs. (A11) and (A12) can be approximated by

$$W \cong -i2 (1 - A) \exp[-i\phi(z_u, z_l)], \quad (\text{A18})$$

where

$$A = R_u R_l \exp[-i2 \phi(z_u, z_l)]. \quad (\text{A19})$$

The approximation that leads to this simple expression for  $W$  rests on the assumption that the WKB amplitude functions can be represented by standard WKB forms, i.e.,  $u = v \cong Q^{-1/2}$ .

Using the first term in the asymptotic expansion of  $H_0^{(2)}(kr)$ , i.e.,

$$H_0^{(2)}(kr) \cong (2/\pi kr)^{1/2} \exp[-i(kr - \pi/4)], \quad (\text{A20})$$

the integral in Eq. (A10) can be expressed in the form

$$\Phi = \int_{-\infty}^{\infty} \sum_{n=1}^4 F_n \exp[-i(\Psi_n + kr)] \frac{dk}{1 - A}, \quad (\text{A21})$$

where the  $F_n$  are given by

$$F_1 = u(z_S) v(z_r) K(kr),$$

$$F_2 = R_U u^*(z_S) v(z_r) K(kr),$$

$$F_3 = R_I u(z_S) v^*(z_r) K(kr),$$

$$\text{and } F_4 = R_U R_I u^*(z_S) v^*(z_r) K(kr), \quad (\text{A22})$$

with  $K(kr) = (k/2\pi r)^{1/2} e^{-i\pi/4}$ , and where the  $\psi_n$  are given by

$$\psi_1 = \phi(z_U, z_I) - \phi(z_U, z_S) - \phi(z_r, z_I),$$

$$\psi_2 = \phi(z_U, z_I) + \phi(z_U, z_S) - \phi(z_r, z_I),$$

$$\psi_3 = \phi(z_U, z_I) - \phi(z_U, z_S) + \phi(z_r, z_I),$$

$$\psi_4 = \phi(z_U, z_I) + \phi(z_U, z_S) + \phi(z_r, z_I). \quad (\text{A23})$$

Thus, the integral, Eq. (A10), has essentially been decomposed into four wave field integrals, each of which can be associated with a ray path that leaves the source in the up or down direction and arrives at the receiver in the up or down direction. The particular identifications are given in the RAYMODE documents of Davis and Council (1985a,b).

Generally,  $U$  and  $V$  assume different forms depending on which side of a turning point depth the field point depth,  $z$ , is located. If the velocity minimum is at a depth falling between the turning point depths, then for  $z_U < z < z_I$  ("allowed" region) these functions are oscillatory, whereas for  $z < z_U$  or  $z > z_I$  ("forbidden" region) they take on exponentially decaying forms. In either of these regions, the amplitude functions,  $u(z)$  and  $v(z)$ , reduce to the standard WKB form, i.e.,  $\sim Q^{-1/2}(z)$ , only when the field point is far removed from a turning point. More generally, however, they are determined iteratively using recurrence relations (Leibiger, 1971).

One of the unique features of RAYMODE is the manner in which the limits of integration are handled. When the integration and summation operations indicated in Eq. (A21) are interchanged, the bulk of the computational effort can be seen to center on integrals of the form

$$I = \int_{-\infty}^{\infty} F(k) e^{-i[\Psi(k) + kr]} \frac{dk}{1 - A(k)}. \quad (\text{A24})$$

Leibiger (1971) recognized that computational economies could be realized by judiciously partitioning the  $k$  axis, assumed to be the real line  $(-\infty, \infty)$ , into several much smaller segments. Thus the integration of Eq. (A24) is performed in a piecewise manner, that is,

$$\int_{-\infty}^{\infty} \longrightarrow \int_{k_m}^{k_{M-\epsilon}} = \int_{k_m}^{k_{n-\epsilon}} + \int_{k_{n+\epsilon}}^{k_{n+1-\epsilon}} + \dots + \int_{k_{n+j-\epsilon}}^{k_{M-\epsilon}} \quad (\text{A25})$$

The set of  $k$  values is first truncated to the interval  $(k_m, k_M)$  which is then further subdivided into segments  $(k_{n+\epsilon}, k_{n+1-\epsilon})$ , where

$$k_m \leq k_{n+\epsilon} < k_{n+1-\epsilon} \leq k_M,$$

and  $\epsilon$  is an arbitrarily small parameter introduced to ensure the integrity of the subsegments. The selection of  $k_m, k_M$  and the further segmentation of  $(k_m, k_M)$  is discussed in some detail in Davis and Council (1985b), who consider a three-duct profile, and in Deavenport (1978), who considers a classical deep-ocean profile containing a surface duct. In his discussion of integration limits, Deavenport notes that (referring to a previous version of RAYMODE) surface duct situations are subjected to special considerations based on complex  $k$  values. These considerations are reviewed in Section III (and Appendix E).

For a given  $k$ -segment, say  $k_a$  to  $k_b$ , the integrals take the form

$$I(k_a, k_b) = \int_{k_a}^{k_b} F(k) e^{-i[\Psi(k) + kr]} \frac{dk}{1 - A(k)}. \quad (\text{A26})$$

When the number of  $k$  values is not excessive,† the integrals are evaluated using normal mode theory. The eigenvalues required in the mode sum are determined by solving

$$1 - A(k_m) = 1 - R_u R_l \exp(-i2\phi_m) = 0, \quad (\text{A27})$$

where  $\phi_m \equiv \phi(z_u, z_l)$ , and the turning point depths  $z_u$  and  $z_l$  correspond to mode  $m$ . Equation (A27) can be expressed as

$$1 - |R_u| e^{i\delta\phi_u} |R_l| e^{i\delta\phi_l} e^{-i2\phi_m} = 0. \quad (\text{A28})$$

The terms  $\delta\phi_u$  and  $\delta\phi_l$  are phase changes that occur at the upper and lower turning points. Representing  $\phi_m$  as a complex quantity with real part denoted by  $\bar{\phi}_m$  and (small) imaginary part denoted by  $\beta_m$ , the real and imaginary components of Eq. (A28) are given by

$$\text{(real part)} \quad 1 - |R_u R_l| e^{2\beta_m} \cos(\delta\phi_u + \delta\phi_l - 2\bar{\phi}_m) = 0, \quad (\text{A29})$$

and

$$\text{(imag part)} \quad |R_u R_l| e^{2\beta_m} \sin(\delta\phi_u + \delta\phi_l - 2\bar{\phi}_m) = 0. \quad (\text{A30})$$

From the imaginary part

$$\delta\phi_u + \delta\phi_l - 2\bar{\phi}_m = 2(m-1)\pi, \quad m = 1, 2, \dots \quad (\text{A31})$$

which implies that  $\cos(\delta\phi_u + \delta\phi_l - \bar{\phi}_m) = 1$ , so that, from the real part,

$$|R_u R_l| = e^{-2\beta_m} = e^{-2\text{Im}\{\phi_m\}}. \quad (\text{A32})$$

By assuming that  $k_m = \bar{k}_m + i\alpha_m$  and that  $\alpha_m (\equiv \text{Im}\{k_m\})$  contributes mainly to modal attenuation, the eigenvalues are taken to be simple poles of the integral (Eq. (A26)) or the zeros of Eq. (A27). Equivalently, the condition expressed by Eq. (A31) may be used if the mode index,  $m$ ,

---

† the maximum number of modes is currently limited to 30 in Passive RAYMODE and 10 in Active RAYMODE

is temporarily treated as a continuous variable. That is, a zero of  $1 - A(k)$  can be found by solving  $d\bar{\phi}_m/dm = \pi$ . Since

$$\frac{d\bar{\phi}_m}{dm} = -\frac{d\bar{k}_m}{dm} \int_{z_u}^{z_1} \bar{k}_m [\omega^2/c^2 - \bar{k}_m^2]^{-1/2} dz, \quad (\text{A33})$$

and since this integral is just the range of a ray proceeding from  $z_u$  to  $z_1$ , corresponding to one-half cycle for mode  $m$ , then

$$\frac{d\bar{\phi}_m}{dm} = -\frac{d\bar{k}_m}{dm} [R_c(\theta_m)/2]. \quad (\text{A34})$$

Thus  $d\bar{k}_m/dm = -2\pi/R_c(\theta_m)$ , where  $R_c(\theta_m)$  is the cycle range for a ray launched with angle  $\theta_m$ . Differentiation of Eq. (A27) w.r.t.  $\bar{k}_m$  -- taking Eq. (A34) into consideration -- yields

$$\left. \frac{\partial}{\partial k_m} (1 - A) \right|_{\bar{k}_m} = -i R_c(\theta_m). \quad (\text{A35})$$

Next the phase factors,  $\phi_m(k)$  and  $\psi_m(k)$ , are approximated by low-order expansions, e.g.,

$$\begin{aligned} \phi_m(k_m) &\cong \phi(\bar{k}_m) + \phi'(\bar{k}_m)(k - \bar{k}_m) \\ &\cong \phi(\bar{k}_m) - 1/2 R_c(\theta_m) \alpha_m. \end{aligned} \quad (\text{A36})$$

These approximations along with the expansion of residues yields the RAYMODE normal mode sum, that is

$$I(k_a, k_b) \cong -2\pi \sum_m \frac{F(\bar{k}_m)}{R_c(m)} e^{-i[\Psi(\bar{k}_m) + \bar{k}_m r]} e^{-\text{Im}(k_m)[r - R_c(m)]}. \quad (\text{A37})$$

where the reflection coefficients have been treated as constants.

When the number of modes is excessive, one of several other approaches can be used in performing the integrations indicated in Eq. (A26). Before one of these other techniques is applied, however, Eq. (A26) is recast into "multipath expansion" form. That is,

$$I(k_a, k_b) = \sum_{n=0}^{\infty} \int_{k_a}^{k_b} |R_u R_l|^n F \exp(-i[\psi + 2n\phi(z_u, z_l) + kr]) dk, \quad (A38)$$

where  $[1 - A(k)]^{-1}$  has been replaced by the infinite series<sup>†</sup>  $\sum A^n(k)$ . This series is convergent for any physical case of interest since  $|A(k)| < 1$ . This stipulation on the magnitude of  $A$  ( $= |R_u R_l|$ ) naturally excludes "perfectly reflecting" boundaries, but, of course, boundaries of this sort do not exist in actual ocean environments. Note that Eq. (A38) is but one of four integrals that comprise the total solution, and, in this regard, the reader is reminded that the forms taken on by  $F$  and  $\psi$  differ slightly from one integral to the next. Using the enumeration scheme of Eq.'s (A22) and (A23), when the reflection coefficient magnitudes,  $|R_u|^n$  and  $|R_l|^n$ , are incorporated into the  $F$ -factors, each  $F$ -factor has  $|R_u|$  raised to the power  $n + p$ , where  $p = 0, 1, 0$  and  $1$ , respectively, and  $|R_l|$  raised to the power  $n + q$ , where  $q = 0, 0, 1$  and  $1$ , respectively.

---

† For an elementary interpretation of this technique consult Sect. 35 in the text by Brekhovskikh (1980).

**Appendix B**  
**Special RAYMODE Integration Methods**

---

The general form of Eq. (A38) is

$$I(k_a, k_b) = \int_{k_a}^{k_b} \beta(k) e^{-i[kr + \alpha(k)]} dk. \quad (B1)$$

An approach often used in the evaluation of integrals of this form is the method of stationary phase. A point of stationary phase occurs at the point  $k^*$ , say, such that the argument of the exponential function -- the phase -- has zero slope. That is,

$$\left. \frac{\partial}{\partial k} [kr + \alpha(k)] \right|_{k^*} = r + \alpha'(k^*) = 0, \quad (B2)$$

where the prime indicates partial differentiation with respect to  $k$ . The contributions to the integral from values of  $k$  outside the interval  $(k^* - \Delta k, k^* + \Delta k)$  tend to cancel due to oscillations in phase, but inside this interval the value of  $kr + \alpha(k)$  is nearly constant.

Following the development of Erdélyi (1956), let  $h(k) = kr + \alpha(k)$  so that Eq. (B1) takes the form

$$I = \int_{k_a}^{k_b} \beta(k) e^{-ih(k)} dk. \quad (B3)$$

If  $k^*$  is a point of stationary phase, then

$$h(k) \cong h(k^*) + \frac{1}{2} h''(k^*) (k - k^*)^2. \quad (B4)$$

Now let  $u^2 = h(k) - h(k^*)$  so that, by implication,

$$u = [h''/2]^{1/2}(k - k^*), \quad (B5)$$

where  $h'' \equiv h''(k)|_{k^*}$ . With this substitution, the above integral, Eq. (B3),

becomes

$$I = \int_{u_1}^{u_2} \frac{2u}{h'(k)} \beta(k) e^{-i[h(k^*) + u^2]} du. \quad (B6)$$

In the neighborhood of  $k^*$ ,  $\beta(k) \rightarrow \beta(k^*)$  and  $2u/h'(k)$  assumes an indeterminate form. Applying L'Hospital's rule

$$2u/h'(k) \rightarrow 2u'/h''(k) \quad (B7)$$

which as  $k \rightarrow k^*$  evaluates to  $(k - k^*)/u = (2/h'')^{1/2}$ , and this result in turn implies that the largest acceptable value for  $\Delta k$  is  $(2/h'')^{1/2}$ . Thus, the integral in Eq. (B6) reduces to

$$I = \beta(k^*) \sqrt{2/h''} e^{-ih(k^*)} \int_{u_1}^{u_2} e^{-iu^2} du. \quad (B8)$$

The variable of integration chosen for RAYMODE is obtained by setting  $y = (2/\pi)^{1/2}u$ , so that Eq. (B8) becomes

$$I = \beta(k^*) \sqrt{\pi/\alpha''(k^*)} e^{-i[\alpha(k^*) + k^*r]} \int_{y_1}^{y_2} e^{-iy^2/2} dy, \quad (B9)$$

which, of course, requires that  $\alpha''(k)$  does not become vanishingly small as  $k \rightarrow k^*$ .

When the point of stationary phase falls outside the segment  $(k_a, k_b)$ , the phase function is expanded about the end-point closest to  $k^*$ . In this case, the Taylor series expansion contains a first-derivative term, but through a suitable transformation the integrand is cast in the same form as the one in Eq. (B9). Thus, in both the illuminated case,  $k^* \in (k_a, k_b)$ , and in the shadow case,  $k^* \notin (k_a, k_b)$ , the integral that has to be

evaluated takes the form

$$I = \int_{y_1}^{y_2} e^{-iy^2/2} dy. \quad (B10)$$

This integral can be expressed in terms of the Fresnel integrals, that is,

$$I = C(y_2) - C(y_1) - i[S(y_2) - S(y_1)], \quad (B11)$$

where

$$C(y) = \int_0^y \cos \frac{\pi}{2} x^2 dx, \quad (B12)$$

and,

$$S(y) = \int_0^y \sin \frac{\pi}{2} x^2 dx. \quad (B13)$$

The limits of integration depend upon the location of  $k^*$  relative to the interval end-points  $k_a$  and  $k_b$ . Leibiger (1971) presents a table of appropriate values of  $y_1$  and  $y_2$  under various conditions on  $k_a - k^*$  and  $k_b - k^*$ .

The special high frequency integration (HFI) method is essentially an extension of the original RAYMODE integration (ORI) method. As shown in Sect. 45 of Brekhovskikh (1980), when  $\alpha''(k^*)$  is finite the integral, Eq. (B1), evaluates to the "saddle point formula" given by

$$I \cong \sqrt{\frac{2\pi}{|\alpha''(k^*)|}} \beta(k^*) e^{-i[\alpha(k^*) \pm \pi/4]}, \quad (B14)$$

where the sign in the exponent agrees with the sign of  $\alpha''(k^*)$ . When  $|\alpha''(k^*)| < \epsilon$ , for some small  $\epsilon > 0$ , the evaluation point  $(r,z)$ , say, is very close to a caustic -- an indication that special handling is required. To cover all possibilities the phase factor,  $\alpha(k) + kr$ , is expanded to an additional term, i.e.,

$$\begin{aligned} \alpha(k) + kr \cong & \alpha(k^*) + k^*r + (\alpha' + r)(k - k^*) \\ & + \alpha''(k - k^*)^2/2 + \alpha'''(k - k^*)^3/6, \end{aligned} \quad (B15)$$

where the derivatives are evaluated at  $k = k^*$ , and  $k^*$  is a point of stationary phase that lies within the interval of integration  $(k_a, k_b)$ . From the stationary phase condition, i.e.,  $\alpha' + r|_{k^*} = 0$ , the  $\alpha$ -derivatives can be expressed in terms of the  $r$ -derivatives. Let  $r_c$  denote the value of range when  $k = k^*$ . Then at  $k = k^*$ ,  $\alpha' = -r_c$ ,  $\alpha'' = -r_c'$  and  $\alpha''' = -r_c''$ . Making these substitutions and assuming that  $\alpha'' \cong 0$ , Eq. (B15) becomes

$$\alpha(k) + kr \cong \alpha(k^*) + k^*r + (r - r_c)(k - k^*) - r_c''(k - k^*)^3/6. \quad (\text{B16})$$

Under these conditions the integral, Eq. (B1), can be put into the form

$$I \cong \beta(k^*) e^{-i[\alpha(k^*) + k^*r]} \\ \times \int \exp\{ i[(r - r_c)(k - k^*) + r_c''(k - k^*)^3/6] \}. \quad (\text{B17})$$

Through suitable transformations applied to the variables  $r - r_c$  and  $k - k^*$  (see, for example, p.390 in Brekhovskikh, 1980), this integral can be approximated by an Airy function.

In addition to the extended Taylor series expansion, there are some subtle differences between this method and the approach taken in the ORI method. In the "original" method, the derivative  $r'$  is determined using finite differences, whereas in the "high frequency" method it is determined analytically. Finite differencing is used in estimating  $r''$  however.

**Appendix C**  
**Breakdown of Phase Factor**

---

The integration procedure identified in the text as the "Original RAYMODE Integration" method is applied to integrals having the form given in Eq. (A38), i.e.,

$$I(k_a, k_b) = \int_{k_a}^{k_b} \beta(k) e^{-i[\alpha(k) + kr]} dk. \quad (C1)$$

This notation conforms with that used by Davis and Council (1985b). Although this notation is convenient, it tends to disguise a feature of some importance concerning the applicability of the stationary phase method. Generally speaking, when the method of stationary phase is applied to integrals of the form

$$I = \int_a^b A(x) e^{i\lambda f(x)} dx, \quad (C2)$$

a fundamental consideration pertains to the amplitude and phase factors  $A(x)$  and  $\lambda f(x)$ . In Eq. (C1) the amplitude factor is a rather involved function of reflection coefficient amplitudes and WKB amplitude functions. Their arguments have been lumped in the factor  $\alpha(k)$ , and this factor tends to "beat against" the factor  $kr$ . Thus, the phase factor in Eq. (C1) goes through positive and negative swings about some mean value, whereas the amplitude factor -- even though fairly complicated -- varies smoothly by comparison. Following procedures similar to those that lead to Eq. (B8), the integral in Eq. (C2) can be approximated by

$$I \cong \sqrt{\frac{2}{\lambda |f''(x_0)|}} A(x_0) e^{i\lambda f(x_0)} \int_{-c\sqrt{\lambda |f''|/2}}^{c\sqrt{\lambda |f''|/2}} e^{\pm iu^2} du, \quad (C3)$$

for any small  $\varepsilon > 0$  (Bleistein and Handelsman, 1986). This approximation improves as  $\varepsilon \rightarrow 0$  and  $\varepsilon\sqrt{\lambda} \rightarrow \infty$ , and if these limits are approached Eq. (C3) can be replaced by

$$I \cong \sqrt{\frac{2\pi}{\lambda |f''(x_0)|}} A(x_0) e^{i[\lambda f(x_0) \pm \pi/4]}, \quad (C4)$$

where  $x_0$  is "the" point of stationary phase and the assignment of + or - corresponds to the sign of  $f''(x_0)$ . Eq. (C4) is referred to as the "stationary phase formula." The analysis that leads to this formula is referred to as the "stationary phase method", and essentially represents a particular approach that falls under the more general heading of "saddle point analysis" (Bleistein and Handelsman, 1986). A tacit assumption made in arriving at this "formula" is that there is only one point of stationary phase falling on the interval of integration.

In an attempt to achieve greater clarity, attention is focused on the  $\alpha$ -component of the phase factor in Eq. (C1). This component takes the form

$$\alpha(k) = \psi + 2n \phi(z_u, z_l), \quad (C5)$$

where

$$\psi = \phi(z_u, z_l) \pm \phi(z_u, z_s) \pm \phi(z_r, z_l). \quad (C6)$$

The  $\phi$  functions are of primary interest here. The reader is reminded that these expressions assume the relationship  $z_u < z_s \leq z_r < z_l$ . Reversing the relationship between  $z_s$  and  $z_r$  results in the same basic expression for  $\psi$  but with the roles of  $z_s$  and  $z_r$  reversed. The  $\phi$  functions are dependent on mode number. Thus, for example, the full expression for  $\phi(z_u, z_s)$  is

$$\phi(z_u, z_s) = \phi_m(z_u, z_s) = \int_{z_u}^{z_s} \sqrt{k^2(z) - k_m^2} dz. \quad (C7)$$

If each wavenumber is multiplied and divided by some reference wave number, say  $k_0$ , this integral takes the form

$$\phi_m(z_u, z_s) = k_0 C_0 \gamma_m(z_u, z_s) = \omega \gamma_m(z_u, z_s), \quad (C8)$$

where

$$\gamma_m(z_u, z_s) = \int_{z_u}^{z_s} \sqrt{C^{-2}(z) - C_m^{-2}} dz, \quad (C9)$$

and  $\omega = 2\pi f$ . Note that  $C_m$  is the "phase" (or ray vertex) velocity, and

hence using Snell's law in the form  $\cos\theta = C(z)/C_m$ , this integral reduces to

$$\gamma_m(z_u, z_s) = \int_{z_u}^{z_s} \frac{\sin\theta}{C(z)} dz, \quad (C10)$$

which is similar to what Smith (1974) refers to as a "characteristic" time. Indeed, using Smith's terminology,  $\gamma_m(z_u, z_l)$  is one-half  $J_m$ , an "adiabatic invariant" for mode  $m$ . Now  $J_m = T_m - R_c(\theta_m)/C_m$ , where  $T_m$  is the modal cycle time,  $C_m$  is the phase (ray vertex) velocity, and  $\omega/C_m = k_m$ , so that the exponential (or phase) factor can be expressed in the form

$$\omega [ (n + 1/2)T_m \pm \gamma_m(z_u, z_s) \pm \gamma_m(z_r, z_l) ] \\ + k_m r - (n + 1/2) k_m R_c(\theta_m). \quad (C11)$$

A specific assignment of the  $\pm$  signs can be associated with a particular "ray" path. The leading term in brackets [ ... ] does not oscillate as range increases. The remaining terms, however, exhibit significant oscillations. These terms can be expressed as

$$k_m [ (k/k_m)r - (n + 1/2) R_c(\theta_m) ]. \quad (C12)$$

Consider the first cycle ( $n = 0$ ) for mode  $m$ . Then, since  $k/k_m$  is close to one, the expression in brackets (Eq. (C12)) is approximately

$$r - R_c(\theta_m)/2, \quad (C13)$$

which as  $r$  varies from zero to  $R_c(\theta_m)$  goes from a value that is negative to one that is positive. Consider the simple case when  $z_s = z_r$ . The mean value of phase for either the "up-up" path or the "down-down" path (i.e.,  $\gamma_m(z_u, z_s)$  and  $\gamma_m(z_r, z_l)$  are equal and opposite in sign and hence cancel) is simply  $\omega T_m/2$ . Thus, the phase oscillates about  $\omega T_m/2$  with swings in amplitude reaching  $\pm R_c(\theta_m)/2$ . Since modal cycle distance increases with increasing

mode number,  $m$ , these oscillations become large in magnitude for high-order modes - although their frequency of oscillation becomes less rapid. Conversely, oscillations for the low-order modes are not as extensive in magnitude but they are fairly rapid. In either case the phase variation is rapid relative to the amplitude variation, and hence as long as the reference wave number  $k_0$  ( $= 2\pi f/C_0$ ) is large, i.e., the frequency is "high", the criteria necessary for Eq. (C4) are met. The validity of Eq. (C3), however, does not necessarily require that  $k_0 \rightarrow \infty$ . Even for relatively modest values of  $k_0$ , as long as the interval of integration is properly confined, this integral yields an acceptable approximation. Obviously there is some frequency below which this method fails. Hopefully the transition to the RAYMODE "normal mode" sum occurs before that frequency is reached!

**Appendix D**  
**Surface Reflection Loss Submodel**

---

The surface loss submodel used in RAYMODE is an ad-hoc adaptation of results derived in part from theoretical considerations and in part from experimental data (Marsh and Schulkin, 1962). That is, the surface loss, SL, is determined from an expression of the form

$$SL = SL_1 + SL_2, \quad (D1)$$

where  $SL_1$  is given by

$$SL_1 = -20 \log (1 - R)^{1/2}, \quad (D2)$$

and where

$$R = \max \{ i \sin\theta, \sin\theta - (\pi a \theta^2)^{-1/2} \exp(-\epsilon a \theta^2) \sin\theta \}. \quad (D3)$$

The parameter  $a$  is related to the mean square slope ( $i \tan^2 \beta_0$ ) through

$$(2a)^{-1} = i \tan^2 \beta_0 = .003 + .0026 V_s, \quad (D4)$$

where  $V_s$  is the 10-meter wind speed in kts (Cox and Munk, 1979). The second term is independent of angle and is given by

$$SL_2 = -10 \log \{ .3 + .7/[1 + .01(2 \times 10^{-5} f V_s^2)^2] \}. \quad (D5)$$

None of the RAYMODE documents offers a derivation of either of these terms. In his evaluation of RAYMODE physics, Deavenport (1979, 1982) notes that the reflection coefficient can be determined from

$$R = 1 - \iint \sigma \cos\phi_r \, d\phi_r \, d\theta_r, \quad (D6)$$

where  $\sigma$  is the scattering coefficient evaluated in the limit of large roughness. This expression is presumably inspired by the works of Beckmann and Spizzichino (1963) and Marsh (1950). Deavenport then notes that  $\sigma$  is proportional to the mean-square scattered power (as given, for example, by Eq. (62), p.89 in Beckmann and Spizzichino., op. cit.). When the indicated integrations are performed, the final form of  $SL_1$  is obtained.

Figure 1 illustrate curves of SL vs.  $\theta$  for frequencies of 1000, 2500, 5000 and 7500 Hz. The three curves in each plot correspond to wind speeds of 5, 15 and 30 kts. Additional remarks pertaining to this submodel may be found in the section on conclusions.

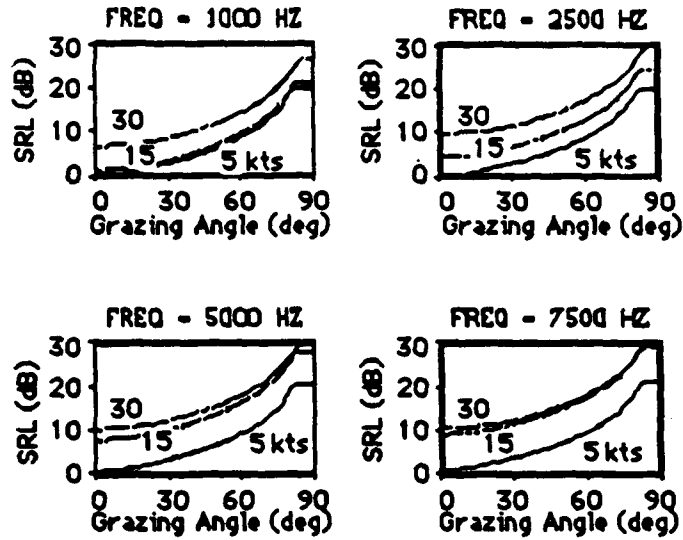


Figure 1. RAYMODE surface reflection loss curves for frequencies of 1, 2.5, 5 and 7.5 KHz and wind speeds of 5, 15 and 30 kts.

**Appendix E**  
**Complex Eigenvalues**

---

Once the appropriate "reflection" coefficients have been determined, the imaginary component of the eigenvalue for mode  $m$  can be approximated by expanding the phase integral, evaluated between turning points, about the real part of  $k_m$ , say  $k_m^*$ , i.e.,

$$\phi(k_m) \cong \phi(k_m^*) + \left. \frac{d\phi(k_m)}{dk_m} \right|_{k_m^*} (k_m - k_m^*), \quad (E1)$$

where,

$$\phi(k_m) = \int_{z_u}^{z_1} \sqrt{[\omega/C(Z)]^2 - k_m^2} dz. \quad (E2)$$

Using the relationship given in Eq. (A34), Eq. (E1) can be expressed as

$$\phi(k_m) \cong \phi(k_m^*) - 1/2 R_c(\theta_m) (k_m - k_m^*). \quad (E3)$$

With  $k_m = k_m^* + i\alpha_m$ , then

$$\phi(k_m) \cong \phi(k_m^*) - iR_c(\theta_m) \alpha_m/2. \quad (E4)$$

Therefore, from Eq. (A32), modal attenuation is given by, approximately,

$$\alpha_m \cong \ln|R_u R_l|/R_c(\theta_m). \quad (E5)$$

For  $Z_s < Z_L$  and  $Z_r < Z_L$ ,  $R_u$  is the surface reflection coefficient and  $R_l$  is the generalized WKB reflection coefficient. For  $Z_s > Z_L$  and  $Z_r > Z_L$ ,  $R_u$  is the generalized WKB reflection coefficient and  $|R_l| = 1$ .

**Appendix F**  
**Departure of  $n^2$ -linear Profile Model from Linearity**

---

Assuming constant salinity, an isothermal BT reading is usually interpreted to indicate that sound velocity varies linearly with depth. To see that the  $n^2$ -linear profile model is generally applicable, consider  $C(Z)$  for  $Z \leq Z_L$ , where the variation in depth is given by,

$$C(Z) = C_0 / (1 - \beta_1 Z)^{1/2}. \quad (F1)$$

The parameter  $\beta_1$  can be determined from a knowledge of the surface sound velocity,  $C_0$ , and the profile point at the layer depth,  $(Z_L, C_L)$ . The velocity gradient  $dC/dZ$ , from Eq. (F1), is given by

$$dC/dZ = 1/2 \beta_1 C^3(Z) / C_0^2, \quad (F2)$$

which at  $Z = Z_L$  is

$$dC/dZ = 1/2 \beta_1 C_L^3 / C_0^2. \quad (F3)$$

Letting  $\Delta C = C_L - C_0$ ,  $\beta_1$  can be determined from

$$\beta_1 = \frac{1 - (C_0/C_L)^2}{Z_L} = \frac{C_L^2 - C_0^2}{Z_L C_L^2} = \frac{(2C_L + \Delta C) \Delta C}{Z_L C_L^2}, \quad (F4)$$

and hence

$$\frac{dC}{dZ} = \frac{\Delta C (2 + \Delta C/C_L)}{2Z_L (1 - \Delta C/Z_L)} \longrightarrow \frac{\Delta C}{Z_L}, \quad (F5)$$

which is just the definition of  $g_1$  for the C-linear (constant gradient) profile model. Thus at  $Z = Z_L$  the ratio, say  $\rho$ , of  $dC/dZ$  for  $n^2$ -linear variation to  $dC/dZ$  for C-linear variation can be expressed as

$$\rho = (C_L/C_0)^3 = \left[ \frac{C_0 + \Delta C}{C_0} \right]^3 = (1 - \Delta C/C_0)^3 \quad (F6)$$

where  $\beta_1$  in Eq. (F3) has been represented as  $2g_1/C_0$ . For  $C_0 = 1500$  m/s and  $\Delta C = 1.8$  m/s, Eq. (F6) yields  $\rho' = 1.0036$ , which suggests that the  $n^2$ -linear model introduces very little curvature.

The usual demonstration of linearity entails expanding the radical in the denominator, that is,

$$C(z) = C_0[1 + 1/2 \beta_1 Z + 3/8 \beta_1^2 Z^2 + \dots ], \quad (F7)$$

which, since  $\beta_1 \ll Z$ , reduces to

$$C(Z) \equiv C_0(1 + 1/2 \beta_1 Z) = C_0 + g_1 Z, \quad (F8)$$

a fairly common form of the C-linear profile model.

**Appendix G**  
**Modal Parameters for a  $C^3$ -linear Duct**

---

The  $C^3$ -linear profile model has a depth dependence given by

$$C^3(Z) = C_0^3(1 + bZ), \quad Z \leq Z_L \quad (G1)$$

where  $b = 3g_0/C_0$  and with  $C_0$  and  $g_0$  denoting sound velocity and its gradient at  $Z = 0$ . The WKB phase integral for a surface duct is given by (see, for example, Freehafer, 1951)

$$\int_C \gamma_m dz = (m - \epsilon) 2\pi, \quad (G2)$$

where  $\gamma_m = [k^2(z) - k_m^2]^{1/2}$ , and where the integration is carried out over a full cycle. Applying Snell's law, this integral can be expressed as

$$\int_C \gamma_m dz = k_m \int_C \tan \theta dz. \quad (G3)$$

Since  $\cos \theta = c/c_m = (c_0/c_m)(1 + bz)^{1/3}$ , then

$$dz = -\frac{3}{b} \left(\frac{c_m}{c_0}\right)^3 \sin \theta \cos^2 \theta d\theta, \quad (G4)$$

so that

$$\begin{aligned} \int_C \gamma_m dz &= -\frac{3}{b} \left(\frac{c_m}{c_0}\right)^3 k_m \int_C \sin^2 \theta \cos \theta d\theta, \\ &= \frac{2\pi f}{3g_0} \left(\frac{c_m}{c_0}\right)^2 \sin^3 \theta + \text{const.} \end{aligned} \quad (G5)$$

The integral over one cycle for "mode"  $m$  is equivalent to twice the integral from  $\theta_0$  ("ray" launch angle) to zero (where "ray" goes horizontal). Assuming that the highest-order trapped mode has turning point depth equal to the layer depth,  $z_L$ , Eq. (G2) takes the form

$$\frac{4\pi f}{3g_0} \frac{\sin^3 \theta_0}{\cos^2 \theta_0} \cong (M - \frac{1}{4}) 2\pi, \quad (G6)$$

or,

$$M \cong \frac{1}{4} + \frac{2}{3} \frac{f}{g_0} \frac{\sin^3 \theta_0}{\cos^2 \theta_0}. \quad (G7)$$

Since  $dr/dz = \cot \theta$  along a ray trajectory, then the cycle distance for "mode"  $m$ , say  $R_c(\theta_m)$ , can be determined from

$$\frac{1}{2} R_c(\theta_m) = \int_{\theta_0}^0 \cot \theta \, dz. \quad (G8)$$

Substituting Eq. (G4) yields

$$\frac{1}{2} R_c(\theta_m) = -\frac{3}{b} \left(\frac{C_L}{C_0}\right)^3 \int_{\theta_0}^0 \cos^3 \theta \, d\theta, \quad (G9)$$

or,

$$\begin{aligned} \frac{1}{2} R_c(\theta_m) &= \frac{3}{b} \left(\frac{C_L}{C_0}\right)^3 \sin \theta_0 \left(1 - \frac{1}{3} \sin^2 \theta_0\right) \\ &= \frac{C_L^3}{C_0^2} \frac{\sin \theta_0}{g_0} \left(1 - \frac{1}{3} \sin^2 \theta_0\right). \end{aligned} \quad (G10)$$

Let  $r_c$  denote cycle distance for the  $n^2$ -linear profile, then (e.g., see McGirr, 1983)

$$\frac{1}{2} r_c(\theta_M) = \frac{C_0}{g_0} \sin \theta_0 \cos \theta_0. \quad (G11)$$

A straight-forward manipulation casts Eq. (G10) into the form

$$\frac{1}{2} R_c(\theta_m) = \left[ \left(\frac{C_L}{C_0}\right)^3 \frac{2 + \cos^2 \theta_0}{3 \cos \theta_0} \right] \frac{1}{2} r_c(\theta_M). \quad (G12)$$

For  $Z_L = 50$  m,  $C_0 = 1500$  m/s and  $C_L = 1501$  m/s, the quantity in square brackets evaluates to 1.00222 -- suggesting that the two profile models produce essentially equivalent "modal" cycle distances.

**Appendix H**  
**Bucker's Scattering Integrals**

---

Bucker (1980) takes surface scattered energy into account by adding randomly-phased scattering terms to the coherent mode sum. He essentially uses ray theory in combination with mode theory to couple surface-scattered energy into the total sound field solution. The additional "mode-to-ray" and "ray-to-mode" interaction terms are incoherently summed to get the total intensity due to the scattered field. The component of intensity due to scattering, say  $I_s$ , is given by

$$I_s = \sum_m [A_m(Z_s)J_m(Z_r) + A_m(Z_r)J_m(Z_s)] \exp(-\alpha_m r), \quad (H1)$$

where  $A_m(Z) = |U_m(Z)/(k_m^{1/2}N_m)|^2$ ,  $\alpha_m = 2 \operatorname{Im}\{k_m\}$ , and

$$J_m = \int [\sigma(\theta_m, \theta_r) \exp(\alpha_m \rho) / \sin \theta_r] d\theta_r, \quad (H2)$$

and where  $\rho = r - r_s$ . The reader interested in specific details pertaining to the various "modal" quantities appearing in these expressions should consult the original article by Bucker (*ibid.*, 1980).

The essential step toward acquiring an appreciation of Bucker's approach is to understand the processes that lead to "scattering" integrals of the form given in Eq. (H2). The intensity associated with the  $m^{\text{th}}$  mode incident on the surface is  $I_m / \cos \theta_m$ . Treating the elemental scattering region of the surface as a point source, the intensity reduction at the receiver is given by

$$f_r^{-1} = \frac{\cos \theta_s / r}{|\sin \theta dr / d\theta_s|}, \quad (H3)$$

where  $f_r$  is what Brekhovskikh (1980) refers to as the focusing factor for a ray launched with angle  $\theta_s$  from the "source." Let  $\sigma$  be the scattering coefficient, then the elemental intensity at the receiver is

$$dI_{sm} = \sigma (I_m / \cos \theta_m) f_r^{-1} r_s dr_s, \quad (H4)$$

or, equating  $\theta_s = \theta_m$ ,

$$f_r^{-1} = \frac{\cos \theta_s / r}{|\sin \theta dr / d\theta_s|}, \quad (H5)$$

Bucker (1980) expresses  $I_m$  in terms of modal quantities, i.e.,

$$I_m = (2\pi/r_s) A_m(z_o) \exp(-\alpha_m r_s), \quad (H6)$$

and then integrates Eq. (H5) to get

$$I_{sm} = (2\pi/r) A_m(z_o) J_m(z) \exp(-\alpha_m r), \quad (H7)$$

where  $J_m(z)$  -- not to be confused with a Bessel function -- is given by Eq. (H2). The limits of integration are defined as the limiting values of the set of rays that directly connect the surface and either the source or the receiver. That is, there are actually two interaction (or scattering) integrals. Near the source, rays propagate energy to the rough surface, whereupon the incoherent component of the surface scattered energy gives rise to normal modes which continue the propagation of waves toward the receiver. This interactive effect represents a ray-to-mode exchange of energy. Near the receiver, the energy associated with a given mode is scattered by the rough surface, whereupon the incoherent component of the surface scattered energy gives rise to rays that propagate energy from the surface to the receiver. This interactive effect represents a mode-to-ray exchange of energy. The details of this procedure are omitted here but may be found in the report by Gordon and Bucker (1984).

In his original article, Bucker (1980) assumes that the specular surface reflection coefficient,  $S_m$ , is given by

$$S_m = -\exp(-g_m/2). \quad (H8)$$

The parameter  $g_m$ , referred to as the Rayleigh roughness parameter, is defined as (e.g., see p. 82 in Beckmann and Spizzichino, 1963)

$$g_m = (2k_s h \sin\theta_{sm})^2, \quad (H9)$$

where  $k_s = \omega/C_s$ ,  $\theta_{sm}$  is the surface grazing angle of incidence for the  $m^{\text{th}}$  mode, and  $h$  is the rms surface roughness. He also assumes Lambert's law (Houston, 1915) which, when the energy lost to specular reflection is taken into account, results in the following expression for  $\sigma$ :

$$\sigma(\theta_m, \theta_s) = 1/2 (1 - |S_m|^2) \sin\theta_s. \quad (H10)$$

### Distribution List

Asst Secretary of the Navy  
(Research, Engineering & Systems)  
Navy Department  
Washington DC 20350-1000

Chief of Naval Operations  
Navy Department  
Washington DC 20350-1000  
Attn: OP-02  
OP-71  
OP-0962X, R. Feden  
OP-987

Oceanographer of the Navy  
Chief of Naval Operations  
U.S. Naval Observatory  
34th & Mass Ave., NW  
Washington DC 20390-1800  
Attn: OP-96

Commander  
Naval Air Development Center  
Warminster PA 18974-5000  
Attn: Code 3031, C. L. Bartberger

Commanding Officer  
Naval Coastal Systems Center  
Panama City FL 32407-5000

Commander  
Space & Naval Warfare Sys Com  
Washington DC 20363-5100  
Attn: Code 361, J. Reeves

Commanding Officer  
Naval Environmental Prediction  
Research Facility  
Monterey CA 93943-5006

Commander  
Naval Facilities Eng Command  
Naval Facilities Eng Command HQ  
200 Stovall St.  
Alexandria VA 22332-2300

Commanding Officer  
Naval Ocean R&D Activity  
Stennis Space Center MS 39529-5004  
Attn: Code 100  
Code 105  
Code 110  
Code 112  
Code 113  
Code 114  
Code 115  
Code 117, J. Hammack  
Code 125EX  
Code 125L (13)  
Code 125P (1)  
Code 200  
Code 210  
Code 211  
Code 220  
Code 221 (5)  
Code 222 (3)  
Code 223 (6)  
Code 224 (3)  
Code 240  
Code 244  
Code 245  
Code 300  
Code 350, D. Hickman  
Code 351, J. Byrnes  
Code 351, J. Braud  
Code 351, M. Lohrenz

Brooke Farquhar  
NORDA Liaison Office  
Crystal Plaza #5, Room 802  
2211 Jefferson Davis Hwy.  
Arlington VA 22202-5000

Commanding Officer  
Naval Research Laboratory  
Washington DC 20375

Director  
Naval Research Laboratory  
Washington DC 20375  
Attn: Code 5160, W. Kuperman

Commander  
Naval Oceanography Command  
Stennis Space Center MS 39529-5000  
Attn: Code N31, CDR F. Zelic

Commanding Officer  
Fleet Numerical Oceanography Center  
Monterey CA 93943-5005  
Attn: LCDR Braunstein  
LCDR Hall  
LCDR Tompkins

Commanding Officer  
Naval Oceanographic Office  
Stennis Space Center MS 39522-5001  
Attn: Code GGAP, B. Mullen  
Code A, J. Depner  
Code 7300, W. Jobst  
Code 9200, L. Bernard  
Code 9210, A. Crumpler

Commander  
Naval Ocean Systems Center  
San Diego CA 92152-5000  
Attn: Code 541, H. Buckner  
Code 541, F. Ryan

Commanding Officer  
ONR Branch Office  
Box 39  
FPO New York NY 09510-0700

Commander  
David W. Taylor Naval Research Center  
Bethesda MD 20084-5000

Commander  
Naval Surface Weapons Center  
Dahlgren VA 22448-5000  
Attn: Library

Commanding Officer  
Naval Underwater Systems Center  
Newport RI 02841-5047

Superintendent  
Naval Postgraduate School  
Monterey CA 93943  
Attn: H. Medwin (Dept./Physics)  
C. Dunlap, (Dept./Oceanography)

Director of Navy Laboratories  
Rm 1062, Crystal Plaza Bldg 5  
Department of the Navy  
Washington DC 20360

Officer in Charge  
New London Laboratory  
Naval Underwater Sys Cen Det  
New London CT 06320  
Attn: Code 33A, B. Cole  
Code 33A3, P. Herstein  
Code 3342, D. Lee  
Code 6091, J. Doeblor  
Code 6091, R. Almeida  
Code 3342, R. Deavenport  
G. Leibiger

Director  
National Ocean Data Center  
WSC1 Room 103  
6001 Executive Blvd.  
Rockville MD 20852  
Attn: G. W. Withee

Director  
Woods Hole Oceanographic Inst  
P.O. Box 32  
Woods Hole MA 02543

University of California  
Scripps Institute of Oceanography  
Marine Physical Laboratory  
P.O. Box 6049  
San Diego CA 92106  
Attn: W. Hodgekiss

Officer in Charge  
Naval Surface Weapons Center Det  
White Oak Laboratory  
10901 New Hampshire Ave.  
Silver Spring MD 20903-5000  
Attn: Code U31, R. Ahlberg  
Library

Commanding Officer  
Fleet Anti-Sub Warfare Training Center,  
Atlantic  
Naval Station  
Norfolk VA 23511-6495

Defense Mapping Agency Sys Cen  
12100 Sunset Hill Rd. #200  
Reston VA 22090-3207  
Attn: SGWN  
Code 10D/10P, Dr. E. Silva  
Mel Wagner  
Ed Danford

Office of Naval Technology  
800 N. Quincy St.  
Arlington VA 22217-5000  
Attn: Code 20, Dr. P. Selwyn  
Code 228, Dr. M. Briscoe  
Code 234, Dr. C. V. Votaw

Office of Naval Research  
800 N. Quincy St.  
Arlington VA 22217-5000  
Attn: Code 10  
Code 10D/10P, Dr. E. Silva  
Code 12  
Code 112, Dr. E. Hartwig  
Code 125, K. W. Lackie

Commander  
Naval Sea Systems Command  
Naval Sea Systems Command HQ  
Washington DC 20362-5101  
Attn: Code 63D3, P. Tiedeman  
Code PMS 411, Dr. E. Estalote  
Code 63R14, A. Franceschetti

Commanding Officer  
Naval Civil Engineering Laboratory  
Port Hueneme CA 93043

Commander  
Naval Air Systems Command  
Naval Air Systems Command HQ  
Washington DC 20361-0001

Pennsylvania State University  
Applied Research Laboratory  
P.O. Box 30  
State College PA 16801

University of Texas at Austin  
Applied Research Laboratories  
P.O. Box 8029  
Austin TX 78713-8029

Johns Hopkins University  
Applied Physics Laboratory  
Johns Hopkins Rd.  
Laurel MD 20707

University of Washington  
Applied Physics Laboratory  
1013 Northeast 40th St.  
Seattle WA 98105

Office of Naval Research  
Field Detachment  
Stennis Space Center MS 39529  
Attn: Code 125, E. Chaika

Commander  
Submarine Development Squadron 12  
Box 70  
Naval Submarine Base  
New London  
Groton CT 06340

R. E. (Ruth) Keenan  
c/o Associated Scientists  
Box 721  
Woods Hole MA 02543

Science Applications  
International, Corp.  
PO Box 2351  
LaJolla CA 92038

Science Applications  
International, Corp.  
1710 Goodridge Drive  
PO Box 1303  
McLean VA 22102  
Attn: Dr. A. Eller

SYNTEK Engineering & Computer  
Systems, Inc.  
2101 East Jefferson Street  
Suite 300  
Attn: B. Scaife

SYNTEK Engineering & Computer  
Systems, Inc.  
2600 Garden Road  
Suite 202  
Monterey CA 93940  
Attn: N. Greenfeldt

Defence Scientific Establishment  
HMNZ Dockyard  
Devonport, Auckland  
New Zealand  
Attn: R. Bannister  
D. Kewley

Defense Technical Information Center  
Cameron Station (12)  
Alexandria VA 22314

# REPORT DOCUMENTATION PAGE

*Form Approved*  
OMB No. 0704-0188

Public reporting burden for this collection of information is estimated to average 1 hour per response, including the time for reviewing instructions, searching existing data sources, gathering and maintaining the data needed, and completing and reviewing the collection of information. Send comments regarding this burden estimate or any other aspect of this collection of information, including suggestions for reducing this burden, to Washington Headquarters Services, Directorate for Information Operations and Reports, 1215 Jefferson Davis Highway, Suite 1204, Arlington, VA 22202-4302, and to the Office of Management and Budget, Paperwork Reduction Project (0704-0188), Washington, DC 20503.

|  |   |   |                                       |
|--|---|---|---------------------------------------|
| <b>1. Agency Use Only (Leave blank).</b>   | <b>2. Report Date.</b><br>January 1990                              | <b>3. Report Type and Dates Covered.</b><br>Final   |                                       |
| <b>4. Title and Subtitle.</b><br><br>An Analysis of Surface-Duct Propagation Loss Modeling in SHARPS   |   | <b>5. Funding Numbers.</b><br><br><i>Program Element No.</i> 980101 (O&M,N)<br><br><i>Project No.</i> 00101<br><br><i>Task No.</i> 120<br><br><i>Accession No.</i> DN256037 |                                       |
| <b>6. Author(s).</b><br><br>Robert W. McGirr   |   | <b>8. Performing Organization Report Number.</b><br><br>NORDA Report 209  |                                       |
| <b>7. Performing Organization Name(s) and Address(es).</b><br><br>Ocean Acoustics and Technology Directorate<br>Naval Ocean Research and Development Activity<br>Stennis Space Center, Mississippi 39529-5004  |   | <b>10. Sponsoring/Monitoring Agency Report Number.</b>  |                                       |
| <b>9. Sponsoring/Monitoring Agency Name(s) and Address(es).</b><br><br>ASW Tactical Support Division<br>Fleet Numerical Oceanography Center<br>Monterey, California 93943  |   | <b>11. Supplementary Notes.</b>   |                                       |
| <b>12a. Distribution/Availability Statement.</b><br><br>Approved for public release; distribution is unlimited. Naval Ocean Research and Development Activity, Stennis Space Center, Mississippi 39529-5004.   |   | <b>12b. Distribution Code.</b>  |                                       |
| <b>13. Abstract (Maximum 200 words).</b><br><br>The propagation submodels of the Ship Helicopter Acoustic Range Prediction System (SHARPS) are reviewed within the context of their effectiveness in making accurate predictions for surface-duct environments. The surface-duct propagation loss calculations performed by SHARPS are based on the submodels contained in Active RAYMODE. Fleet messages have been critical of SHARPS target detection range predictions for in-layer and cross-layer sonar-target geometries. A review is presented of those computational methods—common to both Active and Passive RAYMODE—most likely to affect surface-duct predictions, and includes a summary of the main features of a surface-duct leakage subroutine found in one of the previous versions of Passive RAYMODE. A means of coupling surface-scattered energy into the normal mode sum is reviewed. The possibility of "anomalous" surface-duct predictions is briefly addressed, and several ways to achieve improved surface-duct propagation loss predictions are recommended. |   |   |                                       |
| <b>14. Subject Terms.</b><br><br>underwater acoustics, propagation loss, surface duct, prediction model  |   |   | <b>15. Number of Pages.</b><br><br>85 |
| <b>17. Security Classification of Report.</b><br><br>Unclassified  |   |   | <b>18. Price Code.</b>                |
| <b>18. Security Classification of This Page.</b><br><br>Unclassified   | <b>19. Security Classification of Abstract.</b><br><br>Unclassified | <b>20. Limitation of Abstract.</b><br><br>None  |                                       |